Autonomous Robots manuscript No.
(will be inserted by the editor)

Observability-based Consistent EKF Estimators for Multi-robot Cooperative Localization

Guoquan P. Huang ·
Nikolas Trawny ·
Anastasios I. Mourikis ·
Stergios I. Roumeliotis

Received: date / Accepted: date

Abstract In this paper, we investigate the consistency of extended Kalman filter (EKF)-based cooperative localization (CL) from the perspective of observability. We analytically show that the error-state system model employed in the standard EKF-based CL always has an observable subspace of higher dimension than that of the actual nonlinear CL system. This results in unjustified reduction of the EKF covariance estimates in directions of the state space where no information is available, and thus leads to inconsistency. To address this problem, we adopt an observability-based methodology for designing consistent estimators in which the linearization points are selected to ensure a linearized system model with observable subspace of correct dimension. In particular, we propose two novel observability-constrained (OC)-EKF estimators that are instances of this paradigm. In the first, termed OC-EKF 1.0, the filter Jacobians are calculated using the prior state estimates as the linearization points. In the second, termed OC-EKF 2.0, the linearization points are selected so as to minimize their expected errors (i.e., the difference between the linearization point and the true state) under the observability constraints. The proposed OC-EKFs have been tested in simulation and experimentally, and have been shown to significantly outperform the standard EKF in terms of both accuracy and consistency.

G. P. Huang, N. Trawny and S. I. Roumeliotis
Department of Computer Science and Engineering, University of Minnesota, Minneapolis, MN 55455
E-mail: {ghuang|trawny|stergios}@cs.umn.edu

A. I. Mourikis
Department of Electrical Engineering, University of California, Riverside, CA 92521
E-mail: mourikis@ee.ucr.edu

Keywords Cooperative localization · Nonlinear estimation · Extended Kalman filter · Linearization errors · Estimator inconsistency · Observability

1 Introduction

In order for multi-robot teams to navigate autonomously and successfully perform tasks such as exploration [1], surveillance [2], and search and rescue [3], they must be able to determine their positions and orientations (poses) precisely. In GPS-denied areas and in the absence of robust landmarks, teams of robots can still localize by sharing relative robot-to-robot measurements and jointly estimating their poses [4–6]. Current approaches to solving the cooperative localization (CL) problem, in either centralized or distributed fashion, are based on the extended Kalman filter (EKF) [6], maximum likelihood estimation (MLE) [7], maximum a posteriori (MAP) estimation [8], or particle filtering (PF) [9]. Among these algorithms, the EKF arguably remains a popular choice primarily due to its relatively low computational cost and easy implementation.

While recent research efforts have primarily focused on reducing the computational complexity of EKF-based CL [10–13], the fundamental issue of *consistency* has received little attention. As defined in [14], a state estimator is consistent if the estimation errors are zero-mean, and have covariance smaller than or equal to the one calculated by the filter. Consistency is one of the primary criteria for evaluating the performance of any estimator: if an estimator is inconsistent, then the accuracy of the produced state estimates is unknown, which renders the estimator unreliable.

In our previous work [15], we have studied the consistency of EKF-CL for the case of a two-robot team. Specifically, based on the system observability analysis, we identified a major cause of the inconsistency of the standard EKF-CL and introduced a new EKF estimator that significantly improves consistency as well as accuracy. In this paper, we generalize the analysis of [15] to the case where an arbitrary number of robots comprise the team, and moreover, propose an alternative approach within the same observability-constrained framework to further improve consistency and accuracy. In particular, the major contributions of this work are the following:

- We investigate the observability properties of the error-state system model employed by the EKF, and show that its observable subspace has *higher dimension* than that of the underlying nonlinear CL system. As a result, the covariance estimates of the EKF undergo reduction in directions of the state space where no information is available, hence leading to *inconsistency*. To the best of our knowledge, this work, along with our prior

work [15], is the first to identify and report this inconsistency of the standard EKF-CL.
- Based on the observability analysis, we introduce two new observability-constrained (OC)-EKF estimators, termed OC-EKF 1.0 and OC-EKF 2.0. These two estimators judiciously select the linearization points to ensure that the linearized CL system has an observable subspace of the *same dimension* as that of the nonlinear CL system, and thus improve consistency. Specifically, in the OC-EKF 1.0 algorithm, the state-propagation Jacobians are evaluated at the *prior* state estimates (i.e., *before* instead of after each update), while the measurement Jacobians are computed in the same way as for the standard EKF. In OC-EKF 2.0, the linearization points are selected so as not only to guarantee the desired observability properties, but also to minimize the expected errors of the linearization points (i.e., the difference between the linearization point and the true state). This can be formulated as a constrained minimization problem, whose solution provides the linearization points used for computing the filter Jacobians.
- Through extensive Monte-Carlo simulations and real-world experiments with both *homogeneous* and *heterogeneous* robot teams, we verify that the OC-EKFs outperform the standard EKF in terms of consistency and accuracy, even though they use less accurate state estimates to compute the filter Jacobians (since the linearization points used in the OC-EKFs are, in general, different from the latest, and thus best, state estimates). This result in turn indicates that the observability properties of the system model play a key role in determining the filter's consistency.

The remainder of the paper is organized as follows: After an overview of related work, we present the standard EKF-CL formulation in Section 3. In Section 4, the observability analysis of CL is employed to prove that the standard EKF-CL always has incorrect observability properties and hence is inconsistent. Section 5 describes the proposed OC-EKF estimators and in Sections 6 and 7 the performance of the estimators is compared against that of the standard EKF through Monte-Carlo simulations and real-world experiments. Finally, Section 8 outlines the main conclusions, as well as possible directions of future work.

2 Related Work

To date, theoretical studies on the properties of CL have focused on issues such as initialization [16–19], system observability [20,16,18], accuracy bounds [21,22], and the complexity of deterministic (static) robot network localization [23]. However, to the best of our knowledge, prior to [15], no work has *analytically* examined the consistency of CL. In contrast, recent research has focused on the consistency of EKF-based simultaneous localization and mapping (SLAM) (see [24–31]), showing that the computed state estimates tend to be inconsistent. Specifically, Julier and Uhlmann [24] first observed that when a stationary robot measures the relative position of a new landmark multiple times, the estimated variance of the robot's orientation becomes smaller. Since the observation of a previously unseen feature does not provide any information about the robot's state, this reduction is "artificial" and thus leads to inconsistency. Bailey *et al.* [26] examined several symptoms of the inconsistency of the standard EKF-SLAM algorithm, and argued, based on simulation results, that the uncertainty in the robot orientation is the main cause of inconsistency. Huang and Dissanayake [28] extended the analysis of [24] to the case of a robot observing a landmark from two positions (i.e., the robot observes a landmark, moves and then re-observes the landmark), and proposed a constraint that the filter Jacobians must satisfy to allow for consistent estimation. They also showed that this condition is generally violated, due to the fact that the filter Jacobians at different time instants are computed using different estimates for the same state variables.

In our previous work [29–31], we conducted a theoretical analysis of the EKF-SLAM inconsistency, and identified as a fundamental cause the mismatch between the dimensions of the observable subspaces of the linearized system, employed by the EKF, and the underlying nonlinear system. Furthermore, we introduced the first estimates Jacobian (FEJ)-EKF and observability-constrained (OC)-EKF, which significantly outperform the standard EKF and the robocentric mapping algorithm [25], in terms of both accuracy and consistency. The two proposed estimators were derived by imposing constraints inferred from the system observability analysis. In this work, we extend this new methodology for designing consistent estimators for nonlinear systems to address the inconsistency of EKF-CL.

We should note that a recent publication by Bahr *et al.* [32] addresses a related but different problem, namely the consistency of a distributed CL algorithm due to reuse of information. In the decentralized estimation scheme of [32], the cross-correlations between the state estimates of different robots are not estimated. However, it is well-known that if cross-correlations between robots are not properly taken into account during filter updates, inconsistency can arise [9,6,33]. The algorithm in [32] avoids inconsistency by maintaining a careful record of past robot-to-robot measurement updates. In contrast to the above fully decentralized scenario, in our work the cross-correlation terms are maintained in the filter, and the EKF employed for estimation is optimal, except for the inaccuracies introduced by linearization. Our work focuses on identifying and addressing the cause of inconsistency of this EKF-CL estimator.

3 Standard EKF-based CL

In this section, we present the equations of the 2D EKF-CL formulation with *general* system and measurement models.[1] In the standard formulation of CL, the state vector comprises the N robot poses expressed in the global frame of reference. Thus, at time-step k the state vector is given by

$$\mathbf{x}_k = \begin{bmatrix} \mathbf{x}_{1_k}^T & \cdots & \mathbf{x}_{N_k}^T \end{bmatrix}^T \tag{1}$$

where $\mathbf{x}_{i_k} \triangleq [\mathbf{p}_{i_k}^T \;\; \phi_{i_k}]^T \triangleq [x_{i_k} \;\; y_{i_k} \;\; \phi_{i_k}]^T$ denotes the ith robot pose (position and orientation). In general, EKF-CL recursively evolves in two steps: propagation and update, based on the discrete-time process and measurement models, respectively.

3.1 EKF Propagation

During propagation, each robot integrates its odometry measurements to obtain an estimate of its pose change between two consecutive time steps, which is then employed in the EKF to propagate the robot state estimate. The EKF propagation equations are given by[2]

$$\hat{\mathbf{p}}_{i_{k+1|k}} = \hat{\mathbf{p}}_{i_{k|k}} + \mathbf{C}(\hat{\phi}_{i_{k|k}})\, {}^k\hat{\mathbf{p}}_{i_{k+1}} \tag{2}$$

$$\hat{\phi}_{i_{k+1|k}} = \hat{\phi}_{i_{k|k}} + {}^k\hat{\phi}_{i_{k+1}} \tag{3}$$

for all $i = 1,\ldots,N$. In the above expressions, $\mathbf{C}(\cdot)$ denotes the 2×2 rotation matrix, and ${}^k\hat{\mathbf{x}}_{i_{k+1}} \triangleq [{}^k\hat{\mathbf{p}}_{i_{k+1}}^T \;\; {}^k\hat{\phi}_{i_{k+1}}]^T$ is the odometry-based estimate of the robot's motion between time-steps k and $k+1$, expressed with respect to the robot frame of reference at time instant k. This estimate is corrupted by zero-mean, white Gaussian noise $\mathbf{w}_{i_k} = {}^k\mathbf{x}_{i_{k+1}} - {}^k\hat{\mathbf{x}}_{i_{k+1}}$, with covariance matrix $\mathbf{Q}_k$. Clearly the process model is nonlinear, and can be described by the following generic nonlinear function:

$$\mathbf{x}_{i_{k+1}} = \mathbf{f}(\mathbf{x}_{i_k}, {}^k\hat{\mathbf{x}}_{i_{k+1}} + \mathbf{w}_{i_k}) \tag{4}$$

Linearization of (4) yields the error-state propagation equation:

$$\tilde{\mathbf{x}}_{i_{k+1|k}} \simeq \boldsymbol{\Phi}_{i_k}\tilde{\mathbf{x}}_{i_{k|k}} + \mathbf{G}_{i_k}\mathbf{w}_{i_k} \tag{5}$$

where $\boldsymbol{\Phi}_{i_k}$ and $\mathbf{G}_{i_k}$ are the system state and noise Jacobians, respectively, given by

$$\boldsymbol{\Phi}_{i_k} = \begin{bmatrix} \mathbf{I}_2 & \mathbf{J}\mathbf{C}(\hat{\phi}_{i_{k|k}})\, {}^k\hat{\mathbf{p}}_{i_{k+1}} \\ \mathbf{0}_{1\times 2} & 1 \end{bmatrix} \tag{6}$$

$$= \begin{bmatrix} \mathbf{I}_2 & \mathbf{J}\left(\hat{\mathbf{p}}_{i_{k+1|k}} - \hat{\mathbf{p}}_{i_{k|k}}\right) \\ \mathbf{0}_{1\times 2} & 1 \end{bmatrix} \tag{7}$$

$$\mathbf{G}_{i_k} = \begin{bmatrix} \mathbf{C}(\hat{\phi}_{i_{k|k}}) & \mathbf{0}_{2\times 1} \\ \mathbf{0}_{1\times 2} & 1 \end{bmatrix} \tag{8}$$

with $\mathbf{J} \triangleq \begin{bmatrix} 0 & -1 \\ 1 & 0 \end{bmatrix}$.

By stacking all N robots' error states to create the error state vector for the entire system, we have

$$\begin{aligned} \tilde{\mathbf{x}}_{k+1|k} &\simeq \begin{bmatrix} \boldsymbol{\Phi}_{1_k} & \cdots & \mathbf{0} \\ \vdots & \ddots & \vdots \\ \mathbf{0} & \cdots & \boldsymbol{\Phi}_{N_k} \end{bmatrix} \begin{bmatrix} \tilde{\mathbf{x}}_{1_{k|k}} \\ \vdots \\ \tilde{\mathbf{x}}_{N_{k|k}} \end{bmatrix} + \begin{bmatrix} \mathbf{G}_{1_k} & \cdots & \mathbf{0} \\ \vdots & \ddots & \vdots \\ \mathbf{0} & \cdots & \mathbf{G}_{N_k} \end{bmatrix} \begin{bmatrix} \mathbf{w}_{1_k} \\ \vdots \\ \mathbf{w}_{N_k} \end{bmatrix} \\ &\triangleq \boldsymbol{\Phi}_k\tilde{\mathbf{x}}_{k|k} + \mathbf{G}_k\mathbf{w}_k \end{aligned} \tag{9}$$

Note that the form of the propagation equations presented above is general, and holds for any robot kinematic model (e.g., unicycle, bicycle, or Ackerman model). The specialization to the common case of a unicycle model can be found in Appendix C.

3.2 EKF Update

The measurements used for updates in CL are always a function of the relative pose (i.e., relative position and orientation) of the observed robot j with respect to the observing robot i,

$$\mathbf{z}_k^{(ij)} = \mathbf{h}(\mathbf{x}_{i_k}, \mathbf{x}_{j_k}) + \mathbf{v}_k^{(ij)} = \mathbf{h}\left({}^i\mathbf{x}_{j_k}\right) + \mathbf{v}_k^{(ij)} \tag{10}$$

where

$${}^i\mathbf{x}_{j_k} = \begin{bmatrix} {}^i\mathbf{p}_{j_k} \\ {}^i\phi_{j_k} \end{bmatrix} = \begin{bmatrix} \mathbf{C}^T(\phi_{i_k})(\mathbf{p}_{j_k} - \mathbf{p}_{i_k}) \\ \phi_{j_k} - \phi_{i_k} \end{bmatrix} \tag{11}$$

is the relative pose of the observed robot j with respect to the observing robot i at time-step k, and $\mathbf{v}_k^{(ij)}$ is zero-mean Gaussian noise with covariance $\mathbf{R}_k^{(ij)}$. In this work, we allow $\mathbf{h}$ to be *any* measurement function. For instance, $\mathbf{z}_k^{(ij)}$ can be a direct measurement of relative pose, a pair of distance and bearing measurements, bearing-only measurements from monocular cameras, etc. In general, the measurement function is nonlinear, and hence it is linearized for use in the EKF. The linearized measurement-error equation is given by

$$\begin{aligned} \tilde{\mathbf{z}}_k^{(ij)} &\simeq \begin{bmatrix} \mathbf{0} & \cdots & \mathbf{H}_{i_k}^{(ij)} & \cdots & \mathbf{H}_{j_k}^{(ij)} & \cdots & \mathbf{0} \end{bmatrix} \tilde{\mathbf{x}}_{k|k-1} + \mathbf{v}_k^{(ij)} \\ &\triangleq \mathbf{H}_k^{(ij)}\tilde{\mathbf{x}}_{k|k-1} + \mathbf{v}_k^{(ij)} \end{aligned} \tag{12}$$

[1] For the purpose of the consistency study and in order to simplify the derivations, in this paper we focus on the centralized EKF-CL. Note that a distributed implementation [6] does not alter the system properties.

[2] Throughout this paper the subscript $\ell|k$ refers to the estimate of a quantity at time step ℓ, after all measurements up to time step k have been processed, while the superscript (ij) refers to the relative measurement from robot i to robot j. $\hat{x}$ is used to denote the estimate of a random variable x, while $\tilde{x} = x - \hat{x}$ is the error in this estimate. $\mathbf{0}_{m\times n}$ and $\mathbf{1}_{m\times n}$ denote $m\times n$ matrices of zeros and ones, respectively, while $\mathbf{I}_n$ is the $n\times n$ identity matrix. Finally, we use the concatenated forms $s\phi$ and $c\phi$ to denote the $\sin\phi$ and $\cos\phi$ functions, respectively.

where $\mathbf{H}_{i_k}^{(ij)}$ and $\mathbf{H}_{j_k}^{(ij)}$ are the Jacobians of $\mathbf{h}$ with respect to the ith and jth robot poses, respectively, evaluated at the state estimate $\hat{\mathbf{x}}_{k|k-1}$. Using the chain rule of differentiation, these are computed as

$$\mathbf{H}_{i_k}^{(ij)} = -(\nabla \mathbf{h}_k^{(ij)})\mathbf{A}(\hat{\phi}_{i_{k|k-1}}) \begin{bmatrix} \mathbf{I}_2 & \mathbf{J}(\hat{\mathbf{p}}_{j_{k|k-1}} - \hat{\mathbf{p}}_{i_{k|k-1}}) \\ \mathbf{0}_{1\times 2} & 1 \end{bmatrix} \quad (13)$$

$$\mathbf{H}_{j_k}^{(ij)} = (\nabla \mathbf{h}_k^{(ij)})\mathbf{A}(\hat{\phi}_{i_{k|k-1}}) \quad (14)$$

where $\mathbf{A}(\hat{\phi}_{i_{k|k-1}}) \triangleq \begin{bmatrix} \mathbf{C}^T(\hat{\phi}_{i_{k|k-1}}) & \mathbf{0}_{2\times 1} \\ \mathbf{0}_{1\times 2} & 1 \end{bmatrix}$, and $\nabla \mathbf{h}_k^{(ij)}$ denotes the Jacobian of $\mathbf{h}$ with respect to the relative pose between the ith and jth robots (i.e., with respect to the vector ${}^i\mathbf{x}_{j_k}$), evaluated at the state estimate $\hat{\mathbf{x}}_{k|k-1}$. Appendix C illustrates the specific form of the above expressions in the case of distance and bearing measurements.

4 CL Observability Analysis

In this section, we perform an observability analysis for the EKF-CL system derived in the previous section, and compare its observability properties with those of the underlying nonlinear system. Based on this analysis, we draw conclusions about the consistency of the filter.

By applying the *observability rank condition* for nonlinear systems [34], Martinelli and Siegwart [20] have shown that the nonlinear system of CL in general has three unobservable degrees of freedom, corresponding to the global position and orientation. However, as we show in this section, the unobservable subspace of the linearized error-state model of the standard EKF is generally only of dimension two, which leads to inconsistency.[3]

Recall that the Jacobian matrices $\mathbf{\Phi}_k$, $\mathbf{G}_k$, and $\mathbf{H}_k$ used in the EKF-CL linearized error-state model (see (9) and (12)), in general, are defined as

$$\mathbf{\Phi}_k = \nabla_{\mathbf{x}_k}\mathbf{f}\Big|_{\{\mathbf{x}^\star_{k|k},\mathbf{x}^\star_{k+1|k},\mathbf{0}\}} \quad (15)$$

$$\mathbf{G}_k = \nabla_{\mathbf{w}_k}\mathbf{f}\Big|_{\{\mathbf{x}^\star_{k|k},\mathbf{0}\}} \quad (16)$$

$$\mathbf{H}_k = \nabla_{\mathbf{x}_k}\mathbf{h}\Big|_{\{\mathbf{x}^\star_{k|k-1}\}} \quad (17)$$

[3] For simplicity, in our analysis we assume that the relative measurements guarantee observability of the relative poses between all robots. For instance, we exclude special cases where the robots' trajectories give rise to additional unobservable modes (e.g., robots moving exactly in parallel or in a straight line [16]). Another case not considered here is that of the robots measuring relative orientation, $(\phi_j - \phi_i)$, *only*. In this case the nonlinear system has $2N+1$ unobservable degrees of freedom [20]. Moreover, since the relative-orientation measurement model is *linear* in the system state, the problems caused by linearization, described in Section 4.2, do not appear in this case.

In these expressions, $\mathbf{x}^\star_{k|k-1}$ and $\mathbf{x}^\star_{k|k}$ denote the *linearization points* for the state $\mathbf{x}_k$, used for evaluating the Jacobians before and after the EKF update at time-step k, respectively. A linearization point equal to the zero vector is chosen for the noise. The EKF employs the linearized system model defined by (9), (12), and (15)-(17) for propagating and updating the state and covariance estimates, and thus the observability properties of this model affect the performance of the estimator.

Since the linearized error-state model of EKF-CL is time-varying, we employ the *local observability matrix* [35] to perform the observability analysis. Specifically, the local observability matrix for the time interval between time-steps k_o and k_o+m is defined by

$$\mathbf{M} \triangleq \begin{bmatrix} \mathbf{H}_{k_o} \\ \mathbf{H}_{k_o+1}\mathbf{\Phi}_{k_o} \\ \vdots \\ \mathbf{H}_{k_o+m}\mathbf{\Phi}_{k_o+m-1}\cdots\mathbf{\Phi}_{k_o} \end{bmatrix} \quad (18)$$

$$= \mathbf{M}(\mathbf{x}^\star_{k_o|k_o-1}, \mathbf{x}^\star_{k_o|k_o}, \ldots, \mathbf{x}^\star_{k_o+m|k_o+m-1}) \quad (19)$$

The last expression (19), makes explicit the fact that the observability matrix is a function of the linearization points used in computing all the Jacobians within the time interval $[k_o, k_o+m]$. In turn, this implies that *the choice of linearization points affects the observability properties* of the linearized error-state system of the EKF. This key fact is the basis of our analysis. In what follows, we discuss different possible choices for linearization, and the observability properties of the corresponding linearized systems.

4.1 Ideal EKF-CL

Before considering the rank of the matrix $\mathbf{M}$, which is constructed using the *estimated* values of the state in the filter Jacobians, it is interesting to study the observability properties of the "oracle", or "ideal" EKF (i.e., the filter whose Jacobians are evaluated using the *true* values of the state variables, so that $\mathbf{x}^\star_{k|k-1} = \mathbf{x}^\star_{k|k} = \mathbf{x}_k$, for all k). In the following, all matrices evaluated using the true state values are denoted by the symbol "$\check{}$".

To make the notation more compact, we define

$$\boldsymbol{\delta}\mathbf{p}_{ij}(k,\ell) \triangleq \mathbf{p}_{i_k} - \mathbf{p}_{j_\ell} \quad (20)$$

which is the difference between two robots' positions at time-steps k and ℓ. Using the above definition, we note that (see (7))

$$\check{\mathbf{\Phi}}_{i_{k_o+1}}\check{\mathbf{\Phi}}_{i_{k_o}} = \begin{bmatrix} \mathbf{I}_2 & \mathbf{J}\boldsymbol{\delta}\mathbf{p}_{ii}(k_o+2,k_o) \\ \mathbf{0}_{1\times 2} & 1 \end{bmatrix} \quad (21)$$

Based on this identity, it is easy to show by induction that

$$\check{\mathbf{\Phi}}_{i_{k_o+\ell-1}}\check{\mathbf{\Phi}}_{i_{k_o+\ell-2}}\cdots\check{\mathbf{\Phi}}_{i_{k_o}} = \begin{bmatrix} \mathbf{I}_2 & \mathbf{J}\boldsymbol{\delta}\mathbf{p}_{ii}(k_o+\ell,k_o) \\ \mathbf{0}_{1\times 2} & 1 \end{bmatrix} \quad (22)$$

which holds for all $\ell > 0$.

In the ensuing derivations, it is assumed that every robot continuously observes all other robots in the team during the time interval $[k_o,\ k_o+m]$, i.e., the relative-measurement graph (RMG) is complete. Note that this assumption is made only to simplify the notation, and is not necessary in the analysis. We hereafter first study the case where two robots comprise the team, and then extend the analysis to the general case in which the group consists of $N > 2$ robots.

4.1.1 Two-robot case

Based on the assumption of a complete RMG, two measurements, $\mathbf{z}^{(12)}_{k_o+\ell}$ and $\mathbf{z}^{(21)}_{k_o+\ell}$, are available at time-step $k_o+\ell$. Thus, the measurement Jacobian $\check{\mathbf{H}}_{k_o+\ell}$ in this case can be written as (see (12)-(14))

$$\check{\mathbf{H}}_{k_o+\ell} = \begin{bmatrix} \check{\mathbf{H}}^{(12)}_{k_o+\ell} \\ \check{\mathbf{H}}^{(21)}_{k_o+\ell} \end{bmatrix} = \begin{bmatrix} \check{\mathbf{H}}^{(12)}_{1_{k_o+\ell}} & \check{\mathbf{H}}^{(12)}_{2_{k_o+\ell}} \\ \check{\mathbf{H}}^{(21)}_{1_{k_o+\ell}} & \check{\mathbf{H}}^{(21)}_{2_{k_o+\ell}} \end{bmatrix} = \tag{23}$$
$$-\mathbf{Diag}\left((\nabla\check{\mathbf{h}}^{(12)}_{k_o+\ell})\mathbf{A}(\phi_{1_{k_o+\ell}}),\ (\nabla\check{\mathbf{h}}^{(21)}_{k_o+\ell})\mathbf{A}(\phi_{2_{k_o+\ell}})\right)\times$$
$$\begin{bmatrix} \mathbf{I}_2 & \mathbf{J}\boldsymbol{\delta}\mathbf{p}_{21}(k_o+\ell,k_o+\ell) & -\mathbf{I}_2 & \mathbf{0}_{2\times 1} \\ \mathbf{0}_{1\times 2} & 1 & \mathbf{0}_{1\times 2} & -1 \\ -\mathbf{I}_2 & \mathbf{0}_{2\times 1} & \mathbf{I}_2 & \mathbf{J}\boldsymbol{\delta}\mathbf{p}_{12}(k_o+\ell,k_o+\ell) \\ \mathbf{0}_{1\times 2} & -1 & \mathbf{0}_{1\times 2} & 1 \end{bmatrix}$$

where $\mathbf{Diag}(\cdot)$ denotes a block diagonal matrix. On the other hand, the following identity is immediate (see (9) and (22)):

$$\check{\boldsymbol{\Phi}}_{k_o+\ell-1}\check{\boldsymbol{\Phi}}_{k_o+\ell-2}\cdots\check{\boldsymbol{\Phi}}_{k_o} =$$
$$\mathbf{Diag}\left(\check{\boldsymbol{\Phi}}_{1_{k_o+\ell-1}}\cdots\check{\boldsymbol{\Phi}}_{1_{k_o}},\ \check{\boldsymbol{\Phi}}_{2_{k_o+\ell-1}}\cdots\check{\boldsymbol{\Phi}}_{2_{k_o}}\right) =$$
$$\begin{bmatrix} \mathbf{I}_2 & \mathbf{J}\boldsymbol{\delta}\mathbf{p}_{11}(k_o+\ell,k_o) & \mathbf{0}_{2\times 2} & \mathbf{0}_{2\times 1} \\ \mathbf{0}_{1\times 2} & 1 & \mathbf{0}_{1\times 2} & 0 \\ \mathbf{0}_{2\times 2} & \mathbf{0}_{2\times 1} & \mathbf{I}_2 & \mathbf{J}\boldsymbol{\delta}\mathbf{p}_{22}(k_o+\ell,k_o) \\ \mathbf{0}_{1\times 2} & 0 & \mathbf{0}_{1\times 2} & 1 \end{bmatrix} \tag{24}$$

From (23) and (24) we obtain

$$\check{\mathbf{H}}_{k_o+\ell}\check{\boldsymbol{\Phi}}_{k_o+\ell-1}\check{\boldsymbol{\Phi}}_{k_o+\ell-2}\cdots\check{\boldsymbol{\Phi}}_{k_o} = \tag{25}$$
$$-\mathbf{Diag}\left((\nabla\check{\mathbf{h}}^{(12)}_{k_o+\ell})\mathbf{A}(\phi_{1_{k_o+\ell}}),\ (\nabla\check{\mathbf{h}}^{(21)}_{k_o+\ell})\mathbf{A}(\phi_{2_{k_o+\ell}})\right)\ \times$$
$$\begin{bmatrix} \mathbf{I}_2 & \mathbf{J}\boldsymbol{\delta}\mathbf{p}_{21}(k_o+\ell,k_o) & -\mathbf{I}_2 & -\mathbf{J}\boldsymbol{\delta}\mathbf{p}_{22}(k_o+\ell,k_o) \\ \mathbf{0}_{1\times 2} & 1 & \mathbf{0}_{1\times 2} & -1 \\ -\mathbf{I}_2 & -\mathbf{J}\boldsymbol{\delta}\mathbf{p}_{11}(k_o+\ell,k_o) & \mathbf{I}_2 & \mathbf{J}\boldsymbol{\delta}\mathbf{p}_{12}(k_o+\ell,k_o) \\ \mathbf{0}_{1\times 2} & -1 & \mathbf{0}_{1\times 2} & 1 \end{bmatrix}$$

Thus, the observability matrix, $\check{\mathbf{M}}$, can be written as (see (18))

$$\check{\mathbf{M}} = \underbrace{-\mathbf{Diag}\left((\nabla\check{\mathbf{h}}^{(12)}_{k_o})\mathbf{A}(\phi_{1_{k_o}}),\ \cdots,\ (\nabla\check{\mathbf{h}}^{(21)}_{k_o+m})\mathbf{A}(\phi_{2_{k_o+m}})\right)}_{\check{\mathbf{D}}}\ \times \tag{26}$$
$$\underbrace{\begin{bmatrix} \mathbf{I}_2 & \mathbf{J}\boldsymbol{\delta}\mathbf{p}_{21}(k_o,k_o) & -\mathbf{I}_2 & \mathbf{0}_{2\times 1} \\ \mathbf{0}_{1\times 2} & 1 & \mathbf{0}_{1\times 2} & -1 \\ -\mathbf{I}_2 & \mathbf{0}_{2\times 1} & \mathbf{I}_2 & \mathbf{J}\boldsymbol{\delta}\mathbf{p}_{12}(k_o,k_o) \\ \mathbf{0}_{1\times 2} & -1 & \mathbf{0}_{1\times 2} & 1 \\ & & & \\ \mathbf{I}_2 & \mathbf{J}\boldsymbol{\delta}\mathbf{p}_{21}(k_o+1,k_o) & -\mathbf{I}_2 & -\mathbf{J}\boldsymbol{\delta}\mathbf{p}_{22}(k_o+1,k_o) \\ \mathbf{0}_{1\times 2} & 1 & \mathbf{0}_{1\times 2} & -1 \\ -\mathbf{I}_2 & -\mathbf{J}\boldsymbol{\delta}\mathbf{p}_{11}(k_o+1,k_o) & \mathbf{I}_2 & \mathbf{J}\boldsymbol{\delta}\mathbf{p}_{12}(k_o+1,k_o) \\ \mathbf{0}_{1\times 2} & -1 & \mathbf{0}_{1\times 2} & 1 \\ \vdots & \vdots & \vdots & \vdots \\ \mathbf{I}_2 & \mathbf{J}\boldsymbol{\delta}\mathbf{p}_{21}(k_o+m,k_o) & -\mathbf{I}_2 & -\mathbf{J}\boldsymbol{\delta}\mathbf{p}_{22}(k_o+m,k_o) \\ \mathbf{0}_{1\times 2} & 1 & \mathbf{0}_{1\times 2} & -1 \\ -\mathbf{I}_2 & -\mathbf{J}\boldsymbol{\delta}\mathbf{p}_{11}(k_o+m,k_o) & \mathbf{I}_2 & \mathbf{J}\boldsymbol{\delta}\mathbf{p}_{12}(k_o+m,k_o) \\ \mathbf{0}_{1\times 2} & -1 & \mathbf{0}_{1\times 2} & 1 \end{bmatrix}}_{\check{\mathbf{U}}}$$

Lemma 41 *The rank of the observability matrix, $\check{\mathbf{M}}$, of the ideal EKF-CL in the two-robot case, is equal to 3.*

Proof The rank of the product of the matrices $\check{\mathbf{D}}$ and $\check{\mathbf{U}}$ is given by (see (4.5.1) in [36])

$$\mathrm{rank}(\check{\mathbf{D}}\check{\mathbf{U}}) = \mathrm{rank}(\check{\mathbf{U}}) - \dim(\mathrm{null}(\check{\mathbf{D}})\bigcap\mathrm{rng}(\check{\mathbf{U}})) \tag{27}$$

where $\mathrm{null}(\cdot)$ denotes the right null space of a matrix, $\mathrm{rng}(\cdot)$ represents the matrix range, and $\dim(\cdot)$ the dimension of a subspace. Denoting $\check{\mathbf{U}} \triangleq \begin{bmatrix}\check{\mathbf{u}}_1 & \cdots & \check{\mathbf{u}}_6\end{bmatrix}$, it is evident that $\check{\mathbf{u}}_1 = -\check{\mathbf{u}}_4$, $\check{\mathbf{u}}_2 = -\check{\mathbf{u}}_5$, while $\check{\mathbf{u}}_3 + \check{\mathbf{u}}_6 = \alpha_1\check{\mathbf{u}}_4 + \alpha_2\check{\mathbf{u}}_5$, where $\mathbf{J}\boldsymbol{\delta}\mathbf{p}_{21}(k_o,k_o) \triangleq -\begin{bmatrix}\alpha_1 \\ \alpha_2\end{bmatrix}$. We also note that $\{\check{\mathbf{u}}_i\}_{i=4}^{6}$ are linearly independent. Therefore, the range of the matrix $\check{\mathbf{U}}$ is spanned by the vectors $\check{\mathbf{u}}_4$, $\check{\mathbf{u}}_5$, and $\check{\mathbf{u}}_6$, i.e.,

$$\mathrm{rng}(\check{\mathbf{U}}) = \underset{\text{col.}}{\mathrm{span}}\begin{bmatrix}\check{\mathbf{u}}_4 & \check{\mathbf{u}}_5 & \check{\mathbf{u}}_6\end{bmatrix} \tag{28}$$

Thus, $\mathrm{rank}(\check{\mathbf{U}}) = 3$. We now observe that in general $\check{\mathbf{D}}\check{\mathbf{u}}_i \neq \mathbf{0}$, for $i = 4,5,6$. Moreover, note that any vector $\mathbf{x} \in \mathrm{rng}(\check{\mathbf{U}}) \setminus \mathbf{0}$ can be written as $\mathbf{x} = \beta_1\check{\mathbf{u}}_4 + \beta_2\check{\mathbf{u}}_5 + \beta_3\check{\mathbf{u}}_6$ for some $\beta_i \in \mathbb{R}$, where β_i, $i = 1,2,3$, are not simultaneously equal to zero. Thus, in general, $\check{\mathbf{D}}\mathbf{x} = \beta_1\check{\mathbf{D}}\check{\mathbf{u}}_4 + \beta_2\check{\mathbf{D}}\check{\mathbf{u}}_5 + \beta_3\check{\mathbf{D}}\check{\mathbf{u}}_6 \neq \mathbf{0}$, which implies that $\mathbf{x}$ does not belong to the null space, $\mathrm{null}(\check{\mathbf{D}})$, of $\check{\mathbf{D}}$. Therefore, $\dim(\mathrm{null}(\check{\mathbf{D}})\bigcap\mathrm{rng}(\check{\mathbf{U}})) = 0$, and, finally, $\mathrm{rank}(\check{\mathbf{M}}) = \mathrm{rank}(\check{\mathbf{U}}) - \dim(\mathrm{null}(\check{\mathbf{D}})\bigcap\mathrm{rng}(\check{\mathbf{U}})) = \mathrm{rank}(\check{\mathbf{U}}) = 3$.

The above lemma shows that three directions of the state space are unobservable. To identify these directions, we examine the null space of the matrix $\check{\mathbf{M}}$. It can be easily verified that a basis for the right null space of $\check{\mathbf{U}}$ (and thus of $\check{\mathbf{M}}$)

is given by

$$\text{null}(\check{\mathbf{M}}) = \underset{\text{col.}}{\text{span}} \begin{bmatrix} \mathbf{I}_2 & \mathbf{J}\mathbf{p}_{1_{k_o}} \\ \mathbf{0}_{1\times 2} & 1 \\ \mathbf{I}_2 & \mathbf{J}\mathbf{p}_{2_{k_o}} \\ \mathbf{0}_{1\times 2} & 1 \end{bmatrix} \triangleq \underset{\text{col.}}{\text{span}} \begin{bmatrix} \mathbf{n}_1 & \mathbf{n}_2 & \mathbf{n}_3 \end{bmatrix} \tag{29}$$

From the structure of the vectors $\mathbf{n}_1$ and $\mathbf{n}_2$ we see that a change in the state by $\Delta\mathbf{x} = \alpha\mathbf{n}_1 + \beta\mathbf{n}_2$, $\alpha, \beta \in \mathbb{R}$ corresponds to a "shifting" of the $x-y$ plane by α units along x, and by β units along y. Thus, if the two robots are shifted equally, the states $\mathbf{x}$ and $\mathbf{x}' = \mathbf{x} + \Delta\mathbf{x}$ will be indistinguishable given the odometry and relative measurements. To understand the physical meaning of $\mathbf{n}_3$, we consider the case where the $x-y$ plane is rotated by a small angle $\delta\phi$. Rotating the coordinate system transforms any point $\mathbf{p} = [x \;\; y]^T$ to a point $\mathbf{p}' = [x' \;\; y']^T$, given by

$$\begin{bmatrix} x' \\ y' \end{bmatrix} = \mathbf{C}(\delta\phi) \begin{bmatrix} x \\ y \end{bmatrix} \simeq \begin{bmatrix} 1 & -\delta\phi \\ \delta\phi & 1 \end{bmatrix} \begin{bmatrix} x \\ y \end{bmatrix} = \begin{bmatrix} x \\ y \end{bmatrix} + \delta\phi \begin{bmatrix} -y \\ x \end{bmatrix}$$

where we have employed the small-angle approximations $c\delta\phi \simeq 1$ and $s\delta\phi \simeq \delta\phi$. Using this result, we see that if the plane containing the two robots is rotated by $\delta\phi$, the CL state vector will change to

$$\mathbf{x}' = \begin{bmatrix} x_1' \\ y_1' \\ \phi_1' \\ x_2' \\ y_2' \\ \phi_2' \end{bmatrix} \simeq \begin{bmatrix} x_1 \\ y_1 \\ \phi_1 \\ x_2 \\ y_2 \\ \phi_2 \end{bmatrix} + \delta\phi \begin{bmatrix} -y_1 \\ x_1 \\ 1 \\ -y_2 \\ x_2 \\ 1 \end{bmatrix} = \mathbf{x} + \delta\phi\mathbf{n}_3 \tag{30}$$

which indicates that the vector $\mathbf{n}_3$ corresponds to a rotation of the $x-y$ plane. This result implies that any such global rotation is unobservable, and will cause no change to the measurements. The preceding analysis for the meaning of the basis vectors of the unobservable subspace agrees with [20] as well as with intuition, which dictates that the *global coordinates* of the state vector (rotation and translation) are unobservable, since the relative measurements only depend on the relative robot configurations.

4.1.2 N-robot case

We now examine the general case where $N > 2$ robots are included in the group. For a complete RMG, the measurement Jacobian matrix at time-step $k_o + \ell$ can be written as

$$\check{\mathbf{H}}_{k_o+\ell} = \tag{31}$$
$$\begin{bmatrix} \check{\mathbf{H}}^{(12)}_{k_o+\ell} \\ \vdots \\ \check{\mathbf{H}}^{(1N)}_{k_o+\ell} \\ \\ \vdots \\ \check{\mathbf{H}}^{(N1)}_{k_o+\ell} \\ \vdots \\ \check{\mathbf{H}}^{(NN-1)}_{k_o+\ell} \end{bmatrix} = \begin{bmatrix} \check{\mathbf{H}}^{(12)}_{1_{k_o+\ell}} & \check{\mathbf{H}}^{(12)}_{2_{k_o+\ell}} & \cdots & 0 & \cdots & 0 & 0 \\ \vdots & \vdots & \ddots & \vdots & \ddots & \vdots & \vdots \\ \check{\mathbf{H}}^{(1N)}_{1_{k_o+\ell}} & 0 & \cdots & 0 & \cdots & 0 & \check{\mathbf{H}}^{(1N)}_{N_{k_o+\ell}} \\ \\ \vdots & \vdots & \ddots & \vdots & \ddots & \vdots & \vdots \\ \check{\mathbf{H}}^{(N1)}_{1_{k_o+\ell}} & 0 & \cdots & 0 & \cdots & 0 & \check{\mathbf{H}}^{(N1)}_{N_{k_o+\ell}} \\ \vdots & \vdots & \ddots & \vdots & \ddots & \vdots & \vdots \\ 0 & 0 & \cdots & 0 & \cdots & \check{\mathbf{H}}^{(NN-1)}_{N-1_{k_o+\ell}} & \check{\mathbf{H}}^{(NN-1)}_{N_{k_o+\ell}} \end{bmatrix}$$

Similarly to (24), the following identity holds:

$$\check{\mathbf{\Phi}}_{k_o+\ell-1}\check{\mathbf{\Phi}}_{k_o+\ell-2}\cdots\check{\mathbf{\Phi}}_{k_o} = \tag{32}$$
$$\mathbf{Diag}\left(\check{\mathbf{\Phi}}_{1_{k_o+\ell-1}}\cdots\check{\mathbf{\Phi}}_{1_{k_o}} \;,\; \cdots \;,\; \check{\mathbf{\Phi}}_{N_{k_o+\ell-1}}\cdots\check{\mathbf{\Phi}}_{N_{k_o}}\right)$$

Therefore, by using the results of (31) and (32), for $\ell = 1, \cdots, m$, and proceeding similarly as in the two-robot case (see (25)), we obtain the observability matrix, $\check{\mathbf{M}}$, shown in (33).

Lemma 42 *The rank of the observability matrix, $\check{\mathbf{M}}$, of the ideal EKF-CL in the general N-robot case, is $3N-3$.*

Proof Proceeding similarly to the proof of Lemma 41, by denoting $\check{\mathbf{U}} \triangleq \begin{bmatrix} \check{\mathbf{u}}_1 & \cdots & \check{\mathbf{u}}_{3N} \end{bmatrix}$, we first note that

$$\check{\mathbf{u}}_1 = -\sum_{i=2}^{N} \check{\mathbf{u}}_{3i-2} \;,\;\; \check{\mathbf{u}}_2 = -\sum_{i=2}^{N} \check{\mathbf{u}}_{3i-1}$$

Our next goal is to show that $\check{\mathbf{u}}_3$ can also be expressed as a linear combination of other columns of $\check{\mathbf{U}}$. We observe that the summation of every third column of the block row of $\check{\mathbf{U}}$ corresponding to robot j measuring robot i at time $k_o + \ell$ is given by

$$\begin{bmatrix} \mathbf{J}\boldsymbol{\delta}\mathbf{p}_{ij}(k_o+\ell, k_o) - \mathbf{J}\boldsymbol{\delta}\mathbf{p}_{ii}(k_o+\ell, k_o) \\ 0 \end{bmatrix} = \begin{bmatrix} \mathbf{J}\boldsymbol{\delta}\mathbf{p}_{ij}(k_o, k_o) \\ 0 \end{bmatrix}$$

We can further decompose the term $\mathbf{J}\boldsymbol{\delta}\mathbf{p}_{ij}(k_o, k_o)$ as

$$\mathbf{J}\boldsymbol{\delta}\mathbf{p}_{ij}(k_o, k_o) = \mathbf{J}\boldsymbol{\delta}\mathbf{p}_{i1}(k_o, k_o) - \mathbf{J}\boldsymbol{\delta}\mathbf{p}_{j1}(k_o, k_o)$$

Using these results, we have

$$\begin{aligned} \sum_{i=1}^{N} \check{\mathbf{u}}_{3i} &= \sum_{i=2}^{N} \alpha_{2i-1}\check{\mathbf{u}}_{3i-2} + \sum_{i=2}^{N} \alpha_{2i}\check{\mathbf{u}}_{3i-1} \\ &= \sum_{i=2}^{N} \begin{bmatrix} \check{\mathbf{u}}_{3i-2} & \check{\mathbf{u}}_{3i-1} \end{bmatrix} \begin{bmatrix} \alpha_{2i-1} \\ \alpha_{2i} \end{bmatrix} \end{aligned}$$

$$\check{\mathbf{M}} = \underbrace{-\mathbf{Diag}\left((\nabla\check{\mathbf{h}}_{k_o}^{(12)})\mathbf{A}(\phi_{1_{k_o}}),\cdots,(\nabla\check{\mathbf{h}}_{k_o+m}^{(NN-1)})\mathbf{A}(\phi_{N_{k_o+m}})\right)}_{\check{\mathbf{D}}} \times \tag{33}$$

$$\underbrace{\begin{bmatrix}
\mathbf{I}_2 & \mathbf{J}\boldsymbol{\delta}\mathbf{p}_{21}(k_o,k_o) & -\mathbf{I}_2 & \mathbf{0}_{2\times1} & \mathbf{0}_{2\times2} & \mathbf{0}_{2\times1} & \cdots & \mathbf{0}_{2\times2} & \mathbf{0}_{2\times1} \\
\mathbf{0}_{1\times2} & 1 & \mathbf{0}_{1\times2} & -1 & \mathbf{0}_{1\times2} & 0 & \cdots & \mathbf{0}_{1\times2} & 0 \\
\mathbf{I}_2 & \mathbf{J}\boldsymbol{\delta}\mathbf{p}_{31}(k_o,k_o) & \mathbf{0}_{2\times2} & \mathbf{0}_{2\times1} & -\mathbf{I}_2 & \mathbf{0}_{2\times1} & \cdots & \mathbf{0}_{2\times2} & \mathbf{0}_{2\times1} \\
\mathbf{0}_{1\times2} & 1 & \mathbf{0}_{1\times2} & 0 & \mathbf{0}_{1\times2} & -1 & \cdots & \mathbf{0}_{1\times2} & 0 \\
\vdots & \vdots & \vdots & \vdots & \vdots & \vdots & \ddots & \vdots & \vdots \\
\mathbf{I}_2 & \mathbf{J}\boldsymbol{\delta}\mathbf{p}_{N1}(k_o,k_o) & \mathbf{0}_{2\times2} & \mathbf{0}_{2\times1} & \mathbf{0}_{2\times2} & \mathbf{0}_{2\times1} & \cdots & -\mathbf{I}_2 & \mathbf{0}_{2\times1} \\
\mathbf{0}_{1\times2} & 1 & \mathbf{0}_{1\times2} & 0 & \mathbf{0}_{1\times2} & 0 & \cdots & \mathbf{0}_{1\times2} & -1 \\
\vdots & \vdots & \vdots & \vdots & \vdots & \vdots & \vdots & \vdots & \vdots \\
-\mathbf{I}_2 & \mathbf{0}_{2\times1} & \mathbf{0}_{2\times2} & \mathbf{0}_{2\times1} & \mathbf{0}_{2\times2} & \mathbf{0}_{2\times1} & \cdots & \mathbf{I}_2 & \mathbf{J}\boldsymbol{\delta}\mathbf{p}_{1N}(k_o,k_o) \\
\mathbf{0}_{1\times2} & -1 & \mathbf{0}_{1\times2} & 0 & \mathbf{0}_{1\times2} & 0 & \cdots & \mathbf{0}_{1\times2} & 1 \\
\mathbf{0}_{2\times2} & \mathbf{0}_{2\times1} & -\mathbf{I}_2 & \mathbf{0}_{2\times1} & \mathbf{0}_{2\times2} & \mathbf{0}_{2\times1} & \cdots & \mathbf{I}_2 & \mathbf{J}\boldsymbol{\delta}\mathbf{p}_{2N}(k_o,k_o) \\
\mathbf{0}_{1\times2} & 0 & \mathbf{0}_{1\times2} & -1 & \mathbf{0}_{1\times2} & 0 & \cdots & \mathbf{0}_{1\times2} & 1 \\
\vdots & \vdots & \vdots & \vdots & \vdots & \vdots & \ddots & \vdots & \vdots \\
\mathbf{0}_{2\times2} & \mathbf{0}_{2\times1} & \mathbf{0}_{2\times2} & \mathbf{0}_{2\times1} & \mathbf{0}_{2\times2} & \mathbf{0}_{2\times1} & \cdots & \mathbf{I}_2 & \mathbf{J}\boldsymbol{\delta}\mathbf{p}_{N-1N}(k_o,k_o) \\
\mathbf{0}_{1\times2} & 0 & \mathbf{0}_{1\times2} & 0 & \mathbf{0}_{1\times2} & 0 & \cdots & \mathbf{0}_{1\times2} & 1 \\
\mathbf{I}_2 & \mathbf{J}\boldsymbol{\delta}\mathbf{p}_{21}(k_o+1,k_o) & -\mathbf{I}_2 & -\mathbf{J}\boldsymbol{\delta}\mathbf{p}_{22}(k_o+1,k_o) & \mathbf{0}_{2\times2} & \mathbf{0}_{2\times1} & \cdots & \mathbf{0}_{2\times2} & \mathbf{0}_{2\times1} \\
\mathbf{0}_{1\times2} & 1 & \mathbf{0}_{1\times2} & -1 & \mathbf{0}_{1\times2} & 0 & \cdots & \mathbf{0}_{1\times2} & 0 \\
\mathbf{I}_2 & \mathbf{J}\boldsymbol{\delta}\mathbf{p}_{31}(k_o+1,k_o) & \mathbf{0}_{2\times2} & \mathbf{0}_{2\times1} & -\mathbf{I}_2 & -\mathbf{J}\boldsymbol{\delta}\mathbf{p}_{33}(k_o+1,k_o) & \cdots & \mathbf{0}_{2\times2} & \mathbf{0}_{2\times1} \\
\mathbf{0}_{1\times2} & 1 & \mathbf{0}_{1\times2} & 0 & \mathbf{0}_{1\times2} & -1 & \cdots & \mathbf{0}_{1\times2} & 0 \\
\vdots & \vdots & \vdots & \vdots & \vdots & \vdots & \ddots & \vdots & \vdots \\
\mathbf{I}_2 & \mathbf{J}\boldsymbol{\delta}\mathbf{p}_{N1}(k_o+1,k_o) & \mathbf{0}_{2\times2} & \mathbf{0}_{2\times1} & \mathbf{0}_{2\times2} & \mathbf{0}_{2\times1} & \cdots & -\mathbf{I}_2 & -\mathbf{J}\boldsymbol{\delta}\mathbf{p}_{NN}(k_o+1,k_o) \\
\mathbf{0}_{1\times2} & 1 & \mathbf{0}_{1\times2} & 0 & \mathbf{0}_{1\times2} & 0 & \cdots & \mathbf{0}_{1\times2} & -1 \\
\vdots & \vdots & \vdots & \vdots & \vdots & \vdots & \vdots & \vdots & \vdots \\
-\mathbf{I}_2 & -\mathbf{J}\boldsymbol{\delta}\mathbf{p}_{11}(k_o+1,k_o) & \mathbf{0}_{2\times2} & \mathbf{0}_{2\times1} & \mathbf{0}_{2\times2} & \mathbf{0}_{2\times1} & \cdots & \mathbf{I}_2 & \mathbf{J}\boldsymbol{\delta}\mathbf{p}_{1N}(k_o+1,k_o) \\
\mathbf{0}_{1\times2} & -1 & \mathbf{0}_{1\times2} & 0 & \mathbf{0}_{1\times2} & 0 & \cdots & \mathbf{0}_{1\times2} & 1 \\
\mathbf{0}_{2\times2} & \mathbf{0}_{2\times1} & -\mathbf{I}_2 & -\mathbf{J}\boldsymbol{\delta}\mathbf{p}_{22}(k_o+1,k_o) & \mathbf{0}_{2\times2} & \mathbf{0}_{2\times1} & \cdots & \mathbf{I}_2 & \mathbf{J}\boldsymbol{\delta}\mathbf{p}_{2N}(k_o+1,k_o) \\
\mathbf{0}_{1\times2} & 0 & \mathbf{0}_{1\times2} & -1 & \mathbf{0}_{1\times2} & 0 & \cdots & \mathbf{0}_{1\times2} & 1 \\
\vdots & \vdots & \vdots & \vdots & \vdots & \vdots & \ddots & \vdots & \vdots \\
\mathbf{0}_{2\times2} & \mathbf{0}_{2\times1} & \mathbf{0}_{2\times2} & \mathbf{0}_{2\times1} & \mathbf{0}_{2\times2} & \mathbf{0}_{2\times1} & \cdots & \mathbf{I}_2 & \mathbf{J}\boldsymbol{\delta}\mathbf{p}_{N-1N}(k_o+1,k_o) \\
\mathbf{0}_{1\times2} & 0 & \mathbf{0}_{1\times2} & 0 & \mathbf{0}_{1\times2} & 0 & \cdots & \mathbf{0}_{1\times2} & 1 \\
\mathbf{I}_2 & \mathbf{J}\boldsymbol{\delta}\mathbf{p}_{21}(k_o+m,k_o) & -\mathbf{I}_2 & -\mathbf{J}\boldsymbol{\delta}\mathbf{p}_{22}(k_o+m,k_o) & \mathbf{0}_{2\times2} & \mathbf{0}_{2\times1} & \cdots & \mathbf{0}_{2\times2} & \mathbf{0}_{2\times1} \\
\mathbf{0}_{1\times2} & 1 & \mathbf{0}_{1\times2} & -1 & \mathbf{0}_{1\times2} & 0 & \cdots & \mathbf{0}_{1\times2} & 0 \\
\mathbf{I}_2 & \mathbf{J}\boldsymbol{\delta}\mathbf{p}_{31}(k_o+m,k_o) & \mathbf{0}_{2\times2} & \mathbf{0}_{2\times1} & -\mathbf{I}_2 & -\mathbf{J}\boldsymbol{\delta}\mathbf{p}_{33}(k_o+m,k_o) & \cdots & \mathbf{0}_{2\times2} & \mathbf{0}_{2\times1} \\
\mathbf{0}_{1\times2} & 1 & \mathbf{0}_{1\times2} & 0 & \mathbf{0}_{1\times2} & -1 & \cdots & \mathbf{0}_{1\times2} & 0 \\
\vdots & \vdots & \vdots & \vdots & \vdots & \vdots & \ddots & \vdots & \vdots \\
\mathbf{I}_2 & \mathbf{J}\boldsymbol{\delta}\mathbf{p}_{N1}(k_o+m,k_o) & \mathbf{0}_{2\times2} & \mathbf{0}_{2\times1} & \mathbf{0}_{2\times2} & \mathbf{0}_{2\times1} & \cdots & -\mathbf{I}_2 & -\mathbf{J}\boldsymbol{\delta}\mathbf{p}_{NN}(k_o+m,k_o) \\
\mathbf{0}_{1\times2} & 1 & \mathbf{0}_{1\times2} & 0 & \mathbf{0}_{1\times2} & 0 & \cdots & \mathbf{0}_{1\times2} & -1 \\
\vdots & \vdots & \vdots & \vdots & \vdots & \vdots & \vdots & \vdots & \vdots \\
-\mathbf{I}_2 & -\mathbf{J}\boldsymbol{\delta}\mathbf{p}_{11}(k_o+m,k_o) & \mathbf{0}_{2\times2} & \mathbf{0}_{2\times1} & \mathbf{0}_{2\times2} & \mathbf{0}_{2\times1} & \cdots & \mathbf{I}_2 & \mathbf{J}\boldsymbol{\delta}\mathbf{p}_{1N}(k_o+m,k_o) \\
\mathbf{0}_{1\times2} & -1 & \mathbf{0}_{1\times2} & 0 & \mathbf{0}_{1\times2} & 0 & \cdots & \mathbf{0}_{1\times2} & 1 \\
\mathbf{0}_{2\times2} & \mathbf{0}_{2\times1} & -\mathbf{I}_2 & -\mathbf{J}\boldsymbol{\delta}\mathbf{p}_{22}(k_o+m,k_o) & \mathbf{0}_{2\times2} & \mathbf{0}_{2\times1} & \cdots & \mathbf{I}_2 & \mathbf{J}\boldsymbol{\delta}\mathbf{p}_{2N}(k_o+m,k_o) \\
\mathbf{0}_{1\times2} & 0 & \mathbf{0}_{1\times2} & -1 & \mathbf{0}_{1\times2} & 0 & \cdots & \mathbf{0}_{1\times2} & 1 \\
\vdots & \vdots & \vdots & \vdots & \vdots & \vdots & \ddots & \vdots & \vdots \\
\mathbf{0}_{2\times2} & \mathbf{0}_{2\times1} & \mathbf{0}_{2\times2} & \mathbf{0}_{2\times1} & \mathbf{0}_{2\times2} & \mathbf{0}_{2\times1} & \cdots & \mathbf{I}_2 & \mathbf{J}\boldsymbol{\delta}\mathbf{p}_{N-1N}(k_o+m,k_o) \\
\mathbf{0}_{1\times2} & 0 & \mathbf{0}_{1\times2} & 0 & \mathbf{0}_{1\times2} & 0 & \cdots & \mathbf{0}_{1\times2} & 1
\end{bmatrix}}_{\check{\mathbf{U}}}$$

where $\begin{bmatrix}\alpha_{2i-1}\\ \alpha_{2i}\end{bmatrix} \triangleq -\mathbf{J}\boldsymbol{\delta}\mathbf{p}_{i1}(k_o,k_o), \forall i=2,\ldots,N$. Now we obtain the desired result

$$\check{\mathbf{u}}_3 = -\sum_{i=2}^{N}\check{\mathbf{u}}_{3i} + \sum_{i=2}^{N}\alpha_{2i-1}\check{\mathbf{u}}_{3i-2} + \sum_{i=2}^{N}\alpha_{2i}\check{\mathbf{u}}_{3i-1}$$

Moreover, we notice that $\{\check{\mathbf{u}}_i\}_{i=4}^{3N}$ are linearly independent. Therefore, the range of the matrix $\check{\mathbf{U}}$ is spanned by its column vectors $\check{\mathbf{u}}_i$, $i=4,\ldots,3N$, i.e.,

$$\text{rng}(\check{\mathbf{U}}) = \underset{\text{col.}}{\text{span}}\begin{bmatrix}\check{\mathbf{u}}_4 & \cdots & \check{\mathbf{u}}_{3N}\end{bmatrix} \tag{34}$$

Thus, $\text{rank}(\check{\mathbf{U}}) = 3N-3$. Analogously, we observe that in general $\check{\mathbf{D}}\check{\mathbf{u}}_i \neq \mathbf{0}$, for $i=4,\ldots,3N$. Moreover, we note that any vector $\mathbf{x}\in\text{rng}(\check{\mathbf{U}})\setminus\mathbf{0}$ can be written as $\mathbf{x}=\sum_{i=1}^{3N-3}\beta_i\check{\mathbf{u}}_{i+3}$ for some $\beta_i\in\mathbb{R}$, where the β_i's are not simultaneously equal to zero. Thus, in general, $\check{\mathbf{D}}\mathbf{x}=\sum_{i=1}^{3N-3}\beta_i\check{\mathbf{D}}\check{\mathbf{u}}_{i+3}\neq\mathbf{0}$, which implies that $\mathbf{x}$ does not belong to the null space, $\text{null}(\check{\mathbf{D}})$, of $\check{\mathbf{D}}$. Therefore, $\dim(\text{null}(\check{\mathbf{D}})\bigcap\text{rng}(\check{\mathbf{U}}))=0$, and, finally, based on the matrix-product rank theorem (see (4.5.1) in [36]), $\text{rank}(\check{\mathbf{M}}) = \text{rank}(\check{\mathbf{U}}) - \dim(\text{null}(\check{\mathbf{D}})\bigcap\text{rng}(\check{\mathbf{U}})) = \text{rank}(\check{\mathbf{U}}) = 3N-3$.

Furthermore, by inspection, a basis for the right null space of $\check{\mathbf{M}}$ is given by

$$\text{null}(\check{\mathbf{M}}) = \underset{\text{col.}}{\text{span}}\begin{bmatrix}\mathbf{I}_2 & \mathbf{J}\mathbf{p}_{1_{k_o}}\\ \mathbf{0}_{1\times2} & 1\\ \mathbf{I}_2 & \mathbf{J}\mathbf{p}_{2_{k_o}}\\ \mathbf{0}_{1\times2} & 1\\ \vdots & \vdots\\ \mathbf{I}_2 & \mathbf{J}\mathbf{p}_{N_{k_o}}\\ \mathbf{0}_{1\times2} & 1\end{bmatrix} \tag{35}$$

Note the similarity of this result with that of (29). Clearly, the physical interpretation of this result is analogous to that of the two-robot case: the global translation and orientation of the state vector are unobservable.

4.2 Standard EKF-CL

We now study the observability properties of the standard EKF-CL, in which the Jacobians are evaluated at the estimated state (i.e., $\mathbf{x}^\star_{k|k-1}=\hat{\mathbf{x}}_{k|k-1}$ and $\mathbf{x}^\star_{k|k}=\hat{\mathbf{x}}_{k|k}$, for all k). Similarly, we begin with the case of a two-robot team, and then generalize to the case where an arbitrary number of robots comprise the group.

We first introduce the following definitions, which will be useful for the ensuing derivations:

$$\mathbf{d}\hat{\mathbf{p}}_i(k) \triangleq \hat{\mathbf{p}}_{i_{k|k}} - \hat{\mathbf{p}}_{i_{k|k-1}} \tag{36}$$

$$\boldsymbol{\Delta}\hat{\mathbf{p}}_{ij}(k,\ell) \triangleq \hat{\mathbf{p}}_{i_{k|k-1}} - \hat{\mathbf{p}}_{j_{k_o|k_o-1}} - \sum_{\tau=k_o}^{\ell}\mathbf{d}\hat{\mathbf{p}}_j(\tau) \tag{37}$$

$$\boldsymbol{\delta}\hat{\mathbf{p}}_{ij}(k,\ell) \triangleq \hat{\mathbf{p}}_{i_{k|k-1}} - \hat{\mathbf{p}}_{j_{\ell|\ell-1}} \tag{38}$$

where k_o is the first time instant of interest, and $k,\ell\geq k_o$. In the above expressions, $\mathbf{d}\hat{\mathbf{p}}_i$ is the correction in the ith robot position estimate due to the EKF update, while $\boldsymbol{\delta}\hat{\mathbf{p}}_{ij}$ is the estimated difference between two robot positions (see (20)) evaluated using the estimates after the respective propagation steps.

4.2.1 Two-robot case

We start by deriving an expression analogous to that of (21), using (7) and the definition of $\boldsymbol{\Delta}\hat{\mathbf{p}}_{ij}$ in (37):

$$\boldsymbol{\Phi}_{i_{k_o+1}}\boldsymbol{\Phi}_{i_{k_o}} = \begin{bmatrix}\mathbf{I}_2 & \mathbf{J}\boldsymbol{\Delta}\hat{\mathbf{p}}_{ii}(k_o+2,k_o+1)\\ \mathbf{0}_{1\times2} & 1\end{bmatrix} \tag{39}$$

Using induction, we can show that

$$\boldsymbol{\Phi}_{i_{k_o+\ell-1}}\boldsymbol{\Phi}_{i_{k_o+\ell-2}}\cdots\boldsymbol{\Phi}_{i_{k_o}} = \begin{bmatrix}\mathbf{I}_2 & \mathbf{J}\boldsymbol{\Delta}\hat{\mathbf{p}}_{ii}(k_o+\ell,k_o+\ell-1)\\ \mathbf{0}_{1\times2} & 1\end{bmatrix}$$

for $\ell>0$. As a result, the following identity is immediate:

$$\boldsymbol{\Phi}_{k_o+\ell-1}\boldsymbol{\Phi}_{k_o+\ell-2}\cdots\boldsymbol{\Phi}_{k_o} = \tag{40}$$
$$\begin{bmatrix}\mathbf{I}_2 & \mathbf{J}\boldsymbol{\Delta}\hat{\mathbf{p}}_{11}(k_o+\ell,k_o+\ell-1) & \mathbf{0}_{2\times2} & \mathbf{0}_{2\times1}\\ \mathbf{0}_{1\times2} & 1 & \mathbf{0}_{1\times2} & 0\\ \mathbf{0}_{2\times2} & \mathbf{0}_{2\times1} & \mathbf{I}_2 & \mathbf{J}\boldsymbol{\Delta}\hat{\mathbf{p}}_{22}(k_o+\ell,k_o+\ell-1)\\ \mathbf{0}_{1\times2} & 0 & \mathbf{0}_{1\times2} & 1\end{bmatrix}$$

The measurement Jacobian now is given by (see (23))

$$\mathbf{H}_{k_o+\ell} = \tag{41}$$
$$-\mathbf{Diag}\Big((\nabla\mathbf{h}^{(12)}_{k_o+\ell})\mathbf{A}(\hat{\phi}_{1_{k_o+\ell|k_o+\ell-1}}),\,(\nabla\mathbf{h}^{(21)}_{k_o+\ell})\mathbf{A}(\hat{\phi}_{2_{k_o+\ell|k_o+\ell-1}})\Big)\times$$
$$\begin{bmatrix}\mathbf{I}_2 & \mathbf{J}\boldsymbol{\delta}\hat{\mathbf{p}}_{21}(k_o+\ell,k_o+\ell) & -\mathbf{I}_2 & \mathbf{0}_{2\times1}\\ \mathbf{0}_{1\times2} & 1 & \mathbf{0}_{1\times2} & -1\\ -\mathbf{I}_2 & \mathbf{0}_{2\times1} & \mathbf{I}_2 & \mathbf{J}\boldsymbol{\delta}\hat{\mathbf{p}}_{12}(k_o+\ell,k_o+\ell)\\ \mathbf{0}_{1\times2} & -1 & \mathbf{0}_{1\times2} & 1\end{bmatrix}$$

Multiplication of (41) and (40) yields

$$\mathbf{H}_{k_o+\ell}\boldsymbol{\Phi}_{k_o+\ell-1}\cdots\boldsymbol{\Phi}_{k_o} = \tag{42}$$
$$-\mathbf{Diag}\Big((\nabla\mathbf{h}^{(12)}_{k_o+\ell})\mathbf{A}(\hat{\phi}_{1_{k_o+\ell|k_o+\ell-1}}),\,(\nabla\mathbf{h}^{(21)}_{k_o+\ell})\mathbf{A}(\hat{\phi}_{2_{k_o+\ell|k_o+\ell-1}})\Big)\times$$
$$\begin{bmatrix}\mathbf{I}_2 & \mathbf{J}\boldsymbol{\Delta}\hat{\mathbf{p}}_{21}(k_o+\ell,k_o+\ell-1) & -\mathbf{I}_2 & -\mathbf{J}\boldsymbol{\Delta}\hat{\mathbf{p}}_{22}(k_o+\ell,k_o+\ell-1)\\ \mathbf{0}_{1\times2} & 1 & \mathbf{0}_{1\times2} & -1\\ -\mathbf{I}_2 & -\mathbf{J}\boldsymbol{\Delta}\hat{\mathbf{p}}_{11}(k_o+\ell,k_o+\ell-1) & \mathbf{I}_2 & \mathbf{J}\boldsymbol{\Delta}\hat{\mathbf{p}}_{12}(k_o+\ell,k_o+\ell-1)\\ \mathbf{0}_{1\times2} & -1 & \mathbf{0}_{1\times2} & 1\end{bmatrix}$$

Thus, the observability matrix $\mathbf{M}$ (see (18)) can be written as

$$\mathbf{M} = \underbrace{-\mathbf{Diag}\left((\nabla\mathbf{h}_{k_o}^{(12)})\mathbf{A}(\hat{\phi}_{1_{k_o|k_o-1}}),\ \cdots,\ (\nabla\mathbf{h}_{k_o+m}^{(21)})\mathbf{A}(\hat{\phi}_{2_{k_o+m|k_o+m-1}})\right)}_{\mathbf{D}} \times \underbrace{\begin{bmatrix} \mathbf{I}_2 & \mathbf{J}\boldsymbol{\delta}\hat{\mathbf{p}}_{21(k_o,k_o)} & -\mathbf{I}_2 & \mathbf{0}_{2\times 1} \\ \mathbf{0}_{1\times 2} & 1 & \mathbf{0}_{1\times 2} & -1 \\ -\mathbf{I}_2 & \mathbf{0}_{2\times 1} & \mathbf{I}_2 & \mathbf{J}\boldsymbol{\delta}\hat{\mathbf{p}}_{12(k_o,k_o)} \\ \mathbf{0}_{1\times 2} & -1 & \mathbf{0}_{1\times 2} & 1 \\ & & & \\ \mathbf{I}_2 & \mathbf{J}\boldsymbol{\Delta}\hat{\mathbf{p}}_{21(k_o+1,k_o)} & -\mathbf{I}_2 & -\mathbf{J}\boldsymbol{\Delta}\hat{\mathbf{p}}_{22(k_o+1,k_o)} \\ \mathbf{0}_{1\times 2} & 1 & \mathbf{0}_{1\times 2} & -1 \\ -\mathbf{I}_2 & -\mathbf{J}\boldsymbol{\Delta}\hat{\mathbf{p}}_{11(k_o+1,k_o)} & \mathbf{I}_2 & \mathbf{J}\boldsymbol{\Delta}\hat{\mathbf{p}}_{12(k_o+1,k_o)} \\ \mathbf{0}_{1\times 2} & -1 & \mathbf{0}_{1\times 2} & 1 \\ \vdots & \vdots & \vdots & \vdots \\ \mathbf{I}_2 & \mathbf{J}\boldsymbol{\Delta}\hat{\mathbf{p}}_{21(k_o+m,k_o+m-1)} & -\mathbf{I}_2 & -\mathbf{J}\boldsymbol{\Delta}\hat{\mathbf{p}}_{22(k_o+m,k_o+m-1)} \\ \mathbf{0}_{1\times 2} & 1 & \mathbf{0}_{1\times 2} & -1 \\ -\mathbf{I}_2 & -\mathbf{J}\boldsymbol{\Delta}\hat{\mathbf{p}}_{11(k_o+m,k_o+m-1)} & \mathbf{I}_2 & \mathbf{J}\boldsymbol{\Delta}\hat{\mathbf{p}}_{12(k_o+m,k_o+m-1)} \\ \mathbf{0}_{1\times 2} & -1 & \mathbf{0}_{1\times 2} & 1 \end{bmatrix}}_{\mathbf{U}} \tag{43}$$

Lemma 43 *The rank of the observability matrix,* $\mathbf{M}$*, of the standard EKF-CL in the two-robot case, is equal to 4.*

Proof We first observe that the EKF update corrections in the robot position estimates, $\mathbf{d}\hat{\mathbf{p}}_i$ (see (36)), are in general different at different time steps. As a consequence, $\boldsymbol{\Delta}\hat{\mathbf{p}}_{ij}$ (see (37)) are also different at different time steps, which means that columns 3 and 6 of matrix $\mathbf{U}$ are general column vectors and thus not linearly dependent on any other columns. Denoting $\mathbf{U} \triangleq \begin{bmatrix}\mathbf{u}_1 \cdots \mathbf{u}_6\end{bmatrix}$, it is evident that $\mathbf{u}_1 = -\mathbf{u}_4$, $\mathbf{u}_2 = -\mathbf{u}_5$, and moreover $\mathbf{u}_4$ and $\mathbf{u}_5$ are linearly independent. Therefore, one possible basis of the range of the matrix $\mathbf{U}$ is its columns vectors $\{\mathbf{u}_i\}_{i=3}^{6}$, i.e., $\text{rng}(\mathbf{U}) = \underset{\text{col.}}{\text{span}}\begin{bmatrix}\mathbf{u}_3 \cdots \mathbf{u}_6\end{bmatrix}$. Therefore, $\text{rank}(\mathbf{U}) = 4$. By proceeding similarly to the proof of Lemma 41, we observe that in general $\mathbf{D}\mathbf{u}_i \neq \mathbf{0}$, for $i = 3,\ldots,6$, and moreover any vector $\mathbf{x} \in \text{rng}(\mathbf{U}) \setminus \mathbf{0}$ can be written as $\mathbf{x} = \sum_{i=1}^{4}\beta_i\mathbf{u}_{i+2}$ for some $\beta_i \in \mathbb{R}$, where the β_i's are not simultaneously equal to zero. As a result, in general, $\mathbf{D}\mathbf{x} = \sum_{i=1}^{4}\beta_i\mathbf{D}\mathbf{u}_{i+2} \neq \mathbf{0}$. Therefore, $\dim(\text{null}(\mathbf{D})\bigcap\text{rng}(\mathbf{U})) = 0$, and finally, based on theorem (4.5.1) in [36], $\text{rank}(\mathbf{M}) = \text{rank}(\mathbf{U}) - \dim(\text{null}(\mathbf{D})\bigcap\text{rng}(\mathbf{U})) = \text{rank}(\mathbf{U}) = 4$.

We thus see that the linearized error-state model employed in the standard EKF-CL has different observability properties than that of the ideal EKF-CL. In particular, by processing the measurements collected in the time interval $[k_o, k_o+m]$, the EKF acquires information along the 4 directions of the state space corresponding to the observable subspace of the linearized system. However, the measurements actually provide information in only 3 directions of the state space (i.e., the robot-to-robot relative pose), and as a result, the EKF gains "spurious information" along the unobservable directions of the underlying nonlinear CL system, which leads to inconsistency.

To probe further, we note that the basis of the right null space of $\mathbf{M}$ is given by

$$\text{null}(\mathbf{M}) = \underset{\text{col.}}{\text{span}}\begin{bmatrix}\mathbf{I}_2 \\ \mathbf{0}_{1\times 2} \\ \mathbf{I}_2 \\ \mathbf{0}_{1\times 2}\end{bmatrix} = \underset{\text{col.}}{\text{span}}\begin{bmatrix}\mathbf{n}_1 & \mathbf{n}_2\end{bmatrix} \tag{44}$$

Note that these two vectors correspond to a shifting of the $x-y$ plane, which implies that such a shifting is unobservable. On the other hand, the direction corresponding to the rotation is "missing" from the unobservable subspace of the EKF system model (see (29) and (30)). Therefore, the filter gains "nonexistent" information about the robots' global orientation. This leads to an unjustified reduction in the orientation uncertainty, which, in turn, further reduces the uncertainty in all state variables.

4.2.2 N-robot case

Similar results can be derived in the general case, where N robots comprise the team. Specifically:

Lemma 44 *The rank of the observability matrix,* $\mathbf{M}$*, of the standard EKF-CL in the general N-robot case, is* $3N-2$*.*

Proof See Appendix A.

We can draw identical conclusions as in the two-robot case. In particular, the dimension of the null space of the observability matrix, $\mathbf{M}$, erroneously becomes 2. Furthermore, one possible basis for the null space can be shown to be

$$\text{null}(\mathbf{M}) = \underset{\text{col.}}{\text{span}}\begin{bmatrix}\mathbf{I}_2 \\ \mathbf{0}_{1\times 2} \\ \vdots \\ \mathbf{I}_2 \\ \mathbf{0}_{1\times 2}\end{bmatrix} \tag{45}$$

Thus, the global orientation is erroneously observable in this case as well, which leads to inconsistent estimates.

5 Observability Constrained (OC)-EKF CL

In the preceding section, it was shown that when the filter Jacobians are evaluated using the latest state estimates, the error-state system model employed by the EKF has an observable subspace of dimension higher than that of the actual CL system. This will always lead to unjustified reduction of the covariance estimates, and thus to inconsistency.

To address this problem, we propose selecting the EKF linearization points in a way that guarantees an unobservable subspace of dimension three for the linearized error-state model. In particular, this corresponds to satisfying conditions (46)-(47) of the following lemma:

Lemma 51 *If the linearization points, $\mathbf{x}^\star_{k|k}$ and $\mathbf{x}^\star_{k+1|k}$, at which the EKF Jacobians $\boldsymbol{\Phi}_k = \boldsymbol{\Phi}_k(\mathbf{x}^\star_{k+1|k}, \mathbf{x}^\star_{k|k})$ and $\mathbf{H}_{k+1} = \mathbf{H}_{k+1}(\mathbf{x}^\star_{k+1|k})$ are evaluated, are selected so as to fulfill the conditions:*

$$\mathbf{H}_{k_o}\mathbf{N} = \mathbf{0}\ , \quad \text{for } \ell = 0 \tag{46}$$

$$\mathbf{H}_{k_o+\ell}\boldsymbol{\Phi}_{k_o+\ell-1}\cdots\boldsymbol{\Phi}_{k_o}\mathbf{N} = \mathbf{0}\ , \quad \forall\, \ell > 0 \tag{47}$$

where $\mathbf{N}$ is a $3N\times 3$ full-rank matrix, then the corresponding observability matrix is of rank $3N-3$.

Proof When (46)-(47) hold, then all the block rows of the observability matrix (see (18)) will have the same null space, spanned by the columns of $\mathbf{N}$.

Essentially, the selection of $\mathbf{N}$ is a design choice, which allows us to control the unobservable subspace of the EKF-CL system model. Ideally, we would like the column vectors of $\mathbf{N}$ to be identical to those in (35), which define the unobservable directions of the ideal EKF-CL system. However, this cannot be achieved in practice, since these directions depend on the *true* values of the state, which are unavailable during any real-world implementation. A natural selection, which is realizable in practice, is to define the unobservable subspace of the observability matrix based on the first available state estimates, i.e., for the two-robot case to choose[4]

$$\mathbf{N} = \underset{\text{col.}}{\text{span}} \begin{bmatrix} \mathbf{I}_2 & \mathbf{J}\hat{\mathbf{p}}_{1_{k_o|k_o-1}} \\ \mathbf{0}_{1\times 2} & 1 \\ \mathbf{I}_2 & \mathbf{J}\hat{\mathbf{p}}_{2_{k_o|k_o-1}} \\ \mathbf{0}_{1\times 2} & 1 \end{bmatrix} \tag{48}$$

Once $\mathbf{N}$ has been selected, the next design decision to be made is the choice of the linearization points at each time step. For the particular selection of $\mathbf{N}$ in (48), this amounts to choosing the linearization points for all $k > k_o$ to ensure that (47) holds (note that (46) is satisfied by construction in this case). Clearly, several options exist, each of which leads to a different algorithm within the general framework described here. In what follows, we extend our prior work [15] and present two algorithms, termed observability-constrained (OC)-EKFs 1.0 and 2.0, to achieve this goal.

[4] When more than two robots (i.e., $N > 2$) are included in the state vector, $\mathbf{N}$ can be chosen analogously, augmented by a submatrix $\begin{bmatrix} \mathbf{I}_2 & \mathbf{J}\hat{\mathbf{p}}_{i_{k_o|k_o-1}} \\ \mathbf{0}_{1\times 2} & 1 \end{bmatrix}$ corresponding to each robot ($i = 1, 2, \ldots, N$) [37].

5.1 OC-EKF 1.0

We start by describing the first version of the OC-EKF (i.e., OC-EKF 1.0) that was originally proposed in our previous work [15]. The key idea of this approach is to choose the prior state estimates as the linearization points, so as to guarantee the appropriate observability properties of the EKF linearized system model. This procedure is explained in detail by the following lemma:

Lemma 52 *If the linearization points, at which the filter Jacobian matrices $\boldsymbol{\Phi}_{i_k} = \boldsymbol{\Phi}_{i_k}(\mathbf{x}^\star_{i_{k+1|k}}, \mathbf{x}^\star_{i_{k|k}})$ and $\mathbf{H}^{(ij)}_k = \mathbf{H}_k(\mathbf{x}^\star_{i_{k|k-1}}, \mathbf{x}^\star_{j_{k|k-1}})$ are evaluated, are selected as*

$$\begin{aligned} &\mathbf{x}^\star_{i_{k+1|k}} = \hat{\mathbf{x}}_{i_{k+1|k}}\ , \quad \mathbf{x}^\star_{i_{k|k}} = \hat{\mathbf{x}}_{i_{k|k-1}} \\ &\mathbf{x}^\star_{i_{k|k-1}} = \hat{\mathbf{x}}_{i_{k|k-1}}\ , \ \mathbf{x}^\star_{j_{k|k-1}} = \hat{\mathbf{x}}_{j_{k|k-1}} \end{aligned} \tag{49}$$

then it is guaranteed that the unobservable subspace of the resulting EKF linearized error-state model is of dimension 3.

Proof Using the linearization points (49), the state-propagation Jacobian $\boldsymbol{\Phi}_{i_k}$ (see (7)) is now computed as

$$\boldsymbol{\Phi}'_{i_k} = \begin{bmatrix} \mathbf{I}_2 & \mathbf{J}\left(\hat{\mathbf{p}}_{i_{k+1|k}} - \hat{\mathbf{p}}_{i_{k|k-1}}\right) \\ \mathbf{0}_{1\times 2} & 1 \end{bmatrix} \tag{50}$$

The difference compared to (7), which is the Jacobian used in the standard EKF, is that the prior estimate of robot position, $\hat{\mathbf{p}}_{i_{k|k-1}}$, is used in place of the posterior estimate, $\hat{\mathbf{p}}_{i_{k|k}}$. In contrast, the measurement Jacobian, $\mathbf{H}^{(ij)}_k$, is computed in the same way as for the standard EKF (see (12)). As a result, using the definition of $\boldsymbol{\delta}\hat{\mathbf{p}}_{ij}$ (38), the observability matrix $\mathbf{M}'$ in the OC-EKF 1.0 algorithm for the two-robot case assumes the following form:

$$\mathbf{M}' = \tag{51}$$

$$\underbrace{-\mathbf{Diag}\left((\nabla\mathbf{h}^{(12)}_{k_o})\mathbf{A}(\hat{\phi}_{1_{k_o|k_o-1}}),\ \cdots,\ (\nabla\mathbf{h}^{(21)}_{k_o+m})\mathbf{A}(\hat{\phi}_{2_{k_o+m|k_o+m-1}})\right)}_{\mathbf{D}'} \times$$

$$\underbrace{\begin{bmatrix} \mathbf{I}_2 & \mathbf{J}\boldsymbol{\delta}\hat{\mathbf{p}}_{21(k_o,k_o)} & -\mathbf{I}_2 & \mathbf{0}_{2\times 1} \\ \mathbf{0}_{1\times 2} & 1 & \mathbf{0}_{1\times 2} & -1 \\ -\mathbf{I}_2 & \mathbf{0}_{2\times 1} & \mathbf{I}_2 & \mathbf{J}\boldsymbol{\delta}\hat{\mathbf{p}}_{12(k_o,k_o)} \\ \mathbf{0}_{1\times 2} & -1 & \mathbf{0}_{1\times 2} & 1 \\ & & & \\ \mathbf{I}_2 & \mathbf{J}\boldsymbol{\delta}\hat{\mathbf{p}}_{21(k_o+1,k_o)} & -\mathbf{I}_2 & -\mathbf{J}\boldsymbol{\delta}\hat{\mathbf{p}}_{22(k_o+1,k_o)} \\ \mathbf{0}_{1\times 2} & 1 & \mathbf{0}_{1\times 2} & -1 \\ -\mathbf{I}_2 & -\mathbf{J}\boldsymbol{\delta}\hat{\mathbf{p}}_{11(k_o+1,k_o)} & \mathbf{I}_2 & \mathbf{J}\boldsymbol{\delta}\hat{\mathbf{p}}_{12(k_o+1,k_o)} \\ \mathbf{0}_{1\times 2} & -1 & \mathbf{0}_{1\times 2} & 1 \\ \vdots & \vdots & \vdots & \vdots \\ \mathbf{I}_2 & \mathbf{J}\boldsymbol{\delta}\hat{\mathbf{p}}_{21(k_o+m,k_o)} & -\mathbf{I}_2 & -\mathbf{J}\boldsymbol{\delta}\hat{\mathbf{p}}_{22(k_o+m,k_o)} \\ \mathbf{0}_{1\times 2} & 1 & \mathbf{0}_{1\times 2} & -1 \\ -\mathbf{I}_2 & -\mathbf{J}\boldsymbol{\delta}\hat{\mathbf{p}}_{11(k_o+m,k_o)} & \mathbf{I}_2 & \mathbf{J}\boldsymbol{\delta}\hat{\mathbf{p}}_{12(k_o+m,k_o)} \\ \mathbf{0}_{1\times 2} & -1 & \mathbf{0}_{1\times 2} & 1 \end{bmatrix}}_{\mathbf{U}'}$$

It becomes evident that compared to the observability matrix of the ideal EKF-CL (see (26)), the only difference arising in $\mathbf{U}'$ is that $\boldsymbol{\delta}\mathbf{p}_{ij}$ is replaced by its estimate, $\boldsymbol{\delta}\hat{\mathbf{p}}_{ij}$, for $i,j=1,2$. Moreover, by inspection, the right null space of $\mathbf{M}'$ is

$$\text{null}(\mathbf{M}') = \underset{\text{col.}}{\text{span}} \begin{bmatrix} \mathbf{I}_2 & \mathbf{J}\hat{\mathbf{p}}_{1_{k_o|k_o-1}} \\ \mathbf{0}_{1\times 2} & 1 \\ \mathbf{I}_2 & \mathbf{J}\hat{\mathbf{p}}_{2_{k_o|k_o-1}} \\ \mathbf{0}_{1\times 2} & 1 \end{bmatrix} \tag{52}$$

Thus, matrix $\mathbf{M}'$ has rank 3, which shows that the OC-EKF 1.0 is based on an error-state system model whose unobservable subspace is of dimension 3. Similarly, in the case where $N>2$ robots comprise the team, it can be easily shown that the corresponding observability matrix $\mathbf{M}'$ follows the same structure as that of the ideal EKF-CL (see (33)), but where $\boldsymbol{\delta}\mathbf{p}_{ij}$ is replaced by its estimate, $\boldsymbol{\delta}\hat{\mathbf{p}}_{ij}$, for all $i,j=1,\ldots,N$. Thus, $\text{rank}(\mathbf{M}')=3N-3$ and the unobservable subspace is of dimension 3 (see [37]).

5.2 OC-EKF 2.0

In the design of consistent estimators for CL, there are two competing goals that should be reconciled: (i) reduced linearization errors at each time step, and (ii) correct observability properties of the linearized system model. In OC-EKF 1.0, the state propagation Jacobian is computed using the predicted estimate $\hat{\mathbf{p}}_{i_{k|k-1}}$ for the robot position instead of the updated, and thus more accurate, estimate $\hat{\mathbf{p}}_{i_{k|k}}$. These two estimates can differ substantially after a large filter correction, which may introduce significant linearization errors. To formally address this limitation, we propose an alternative OC-EKF, termed OC-EKF 2.0, which selects the linearization points of the EKF so as to minimize the expected squared error of the linearization points while satisfying the observability conditions (see (46) and (47)). This can be formulated as a constrained minimization problem where the constraints express the observability requirements.

Specifically, at time-step $k+1$, we aim at minimizing the linearization error of the points $\mathbf{x}^\star_{k|k}$ and $\mathbf{x}^\star_{k+1|k}$, which appear in the filter Jacobians $\boldsymbol{\Phi}_k$ and $\mathbf{H}_{k+1}$ (see (9) and (12), respectively), subject to the observability constraint (47). Mathematically, this is expressed as

$$\min_{\mathbf{x}^\star_{k|k},\, \mathbf{x}^\star_{k+1|k}} \Big(\int \left\|\mathbf{x}_k - \mathbf{x}^\star_{k|k}\right\|^2 p(\mathbf{x}_k|\mathbf{z}_{0:k}) d\mathbf{x}_k + \int \left\|\mathbf{x}_{k+1} - \mathbf{x}^\star_{k+1|k}\right\|^2 p(\mathbf{x}_{k+1}|\mathbf{z}_{0:k}) d\mathbf{x}_{k+1} \Big) \tag{53}$$

$$\text{subject to } \ \mathbf{H}_{k+1}\boldsymbol{\Phi}_k \cdots \boldsymbol{\Phi}_{k_o}\mathbf{N} = \mathbf{0}\,, \ \ \forall k \geq k_o \tag{54}$$

where $\mathbf{z}_{0:k}$ denotes all the measurements available during the time interval $[0,k]$.

In general, the constrained minimization problem (53)-(54) is intractable. However, when the two pdfs, $p(\mathbf{x}_k|\mathbf{z}_{0:k})$ and $p(\mathbf{x}_{k+1}|\mathbf{z}_{0:k})$, are Gaussian distributions (which is the assumption employed in the EKF), we can solve the problem *analytically* and find a closed-form solution. In the following, we show how the closed-form solution can be computed for the simple case where only two robots are included in the state vector. The case of $N>2$ robots is presented in [37].

We note that the following lemma will be helpful for the ensuing derivations:

Lemma 53 *When $p(\mathbf{x}_k|\mathbf{z}_{0:k})$ and $p(\mathbf{x}_{k+1}|\mathbf{z}_{0:k})$ are Gaussian, the constrained optimization problem* (53)-(54) *is equivalent to:*

$$\min_{\mathbf{x}^\star_{k|k},\, \mathbf{x}^\star_{k+1|k}} \left\|\hat{\mathbf{x}}_{k|k} - \mathbf{x}^\star_{k|k}\right\|^2 + \left\|\hat{\mathbf{x}}_{k+1|k} - \mathbf{x}^\star_{k+1|k}\right\|^2 \tag{55}$$

$$\text{subject to } \ \mathbf{p}^\star_{2_{k|k}} - \mathbf{p}^\star_{1_{k|k}} = \mathbf{a}_k \tag{56}$$

where

$$\mathbf{a}_k = \mathbf{p}^\star_{2_{k|k-1}} - \mathbf{p}^\star_{1_{k|k-1}} - \sum_{\tau=k_o}^{k-1} (\mathbf{p}^\star_{2_{\tau|\tau}} - \mathbf{p}^\star_{2_{\tau|\tau-1}}) + \sum_{\tau=k_o}^{k-1} (\mathbf{p}^\star_{1_{\tau|\tau}} - \mathbf{p}^\star_{1_{\tau|\tau-1}})$$

Proof See Appendix B.

Using the technique of Lagrangian multipliers [38], the optimal solution to the problem (55)-(56) can be obtained as

$$\begin{aligned} \mathbf{p}^\star_{1_{k|k}} &= \hat{\mathbf{p}}_{1_{k|k}} + \frac{\boldsymbol{\lambda}_k}{2}\,, \quad \phi^\star_{1_{k|k}} = \hat{\phi}_{1_{k|k}}\,, \\ \mathbf{p}^\star_{2_{k|k}} &= \hat{\mathbf{p}}_{2_{k|k}} - \frac{\boldsymbol{\lambda}_k}{2}\,, \quad \phi^\star_{2_{k|k}} = \hat{\phi}_{2_{k|k}}\,, \\ \mathbf{x}^\star_{k+1|k} &= \hat{\mathbf{x}}_{k+1|k} \end{aligned} \tag{57}$$

with

$$\boldsymbol{\lambda}_k = \hat{\mathbf{p}}_{2_{k|k}} - \hat{\mathbf{p}}_{1_{k|k}} - \mathbf{a}_k$$

We see that $\boldsymbol{\lambda}_k$ and thus the linearization point for the position of each robot, $\mathbf{p}^\star_{i_{k|k}}$, depends on all robots' estimates. This increases the complexity of implementing the algorithm, but yields the optimal linearization errors under the desired observability constraints. Note also that in the case where more than two robots are included in the state vector, each connected robot in the RMG imposes a constraint analogous to (56), and thus the analytical solution of the optimal linearization points can be obtained similarly [37].

Using the linearization points in (57), the state-propagation Jacobians in the OC-EKF 2.0 are now computed as

$$\boldsymbol{\Phi}''_{1_k} = \begin{bmatrix} \mathbf{I}_2 & \mathbf{J}\left(\hat{\mathbf{p}}_{1_{k+1|k}} - \hat{\mathbf{p}}_{1_{k|k}} - \frac{\boldsymbol{\lambda}_k}{2}\right) \\ \mathbf{0}_{1\times 2} & 1 \end{bmatrix} \tag{58}$$

$$\boldsymbol{\Phi}''_{2_k} = \begin{bmatrix} \mathbf{I}_2 & \mathbf{J}\left(\hat{\mathbf{p}}_{2_{k+1|k}} - \hat{\mathbf{p}}_{2_{k|k}} + \frac{\boldsymbol{\lambda}_k}{2}\right) \\ \mathbf{0}_{1\times 2} & 1 \end{bmatrix} \tag{59}$$

while the measurement Jacobians are calculated in the same way as in the standard EKF (see (12)).

It is important to point out that, compared to the standard EKF, the *only* change in the OC-EKFs (1.0 and 2.0) is the way in which the state-propagation Jacobians are computed (see (50), (58), (59) and (7)), while the state estimates and covariance matrices are propagated and updated in the same way as in the standard EKF. For clarity, the steps of the OC-EKF CL algorithm are outlined in Algorithms 1, and a simple CL example with two robots using the unicycle motion model and relative distance and bearing measurements is provided in Appendix C. We also stress that even though a complete RMG (i.e., each robot can observe all others) is assumed at every time step in the preceding analysis, this is not a necessary assumption for the OC-EKF, as the analysis can easily be extended to the case of limited sensor range, where multiple propagation steps occur between updates (see Section 7).

Algorithm 1 Observability Constrained (OC)-EKF CL

Require: Initial state estimates and covariance

loop
  `Propagation:` If odometry information is available,
  propagate the state estimates via (2)-(3)
  if OC-EKF 1.0 **then**
    compute the propagation Jacobian (see (50))
    propagate the state covariance:

$$\mathbf{P}_{k+1|k} = \boldsymbol{\Phi}'_k \mathbf{P}_{k|k} \boldsymbol{\Phi}'^{T}_k + \mathbf{G}_k \mathbf{Q}_k \mathbf{G}^T_k \tag{60}$$

  else if OC-EKF 2.0 **then**
    compute the propagation Jacobian (see (58)-(59))
    propagate the state covariance:

$$\mathbf{P}_{k+1|k} = \boldsymbol{\Phi}''_k \mathbf{P}_{k|k} \boldsymbol{\Phi}''^{T}_k + \mathbf{G}_k \mathbf{Q}_k \mathbf{G}^T_k \tag{61}$$

  end if
  `Update:` If robot-to-robot measurements are available,
  compute the measurement residual:

$$\mathbf{r}_{k+1} = \mathbf{z}_{k+1} - \mathbf{h}(\hat{\mathbf{x}}_{k+1|k}) \tag{62}$$

  compute the measurement Jacobian (see (13)-(14))
  compute the Kalman gain:

$$\mathbf{S}_{k+1} = \mathbf{H}_{k+1} \mathbf{P}_{k+1|k} \mathbf{H}^T_{k+1} + \mathbf{R}_{k+1} \tag{63}$$

$$\mathbf{K}_{k+1} = \mathbf{P}_{k+1|k} \mathbf{H}^T_{k+1} \mathbf{S}^{-1}_{k+1} \tag{64}$$

  update the state estimate and covariance:

$$\hat{\mathbf{x}}_{k+1|k+1} = \hat{\mathbf{x}}_{k+1|k} + \mathbf{K}_{k+1} \mathbf{r}_{k+1} \tag{65}$$

$$\mathbf{P}_{k+1|k+1} = \mathbf{P}_{k+1|k} - \mathbf{K}_{k+1} \mathbf{S}_{k+1} \mathbf{K}^T_{k+1} \tag{66}$$

end loop

As a final remark, we stress that the new OC-EKF estimators are *causal* and *realizable* in practice, since they do not utilize any knowledge of the true state. Interestingly, even though the proposed filters do not use the latest available state estimates (and thus utilize Jacobians that are less accurate than those of the standard EKF), they exhibit better consistency properties than the standard EKF. This is shown through extensive simulations and real-world experiments in the next two sections.

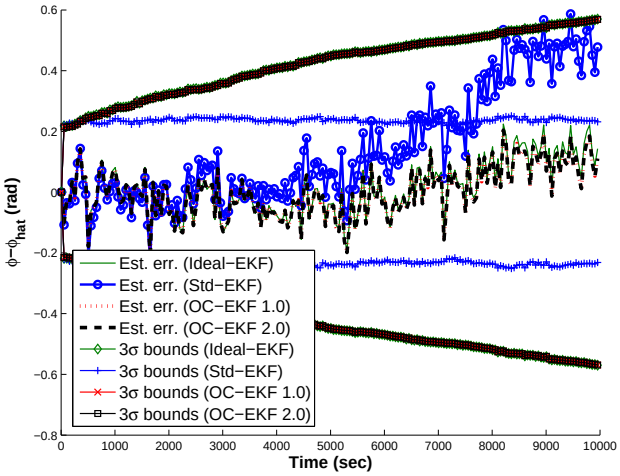

Fig. 1 Orientation estimation errors vs. 3σ bounds for one robot of the 4-robot team, obtained from one typical realization of the Monte Carlo simulations. The results for the other robots are similar to the ones presented here. The σ values are computed as the square-root of the corresponding element of the estimated covariance matrix. Note that the estimation errors as well as the 3σ bounds of the ideal and the OC-EKFs are almost identical, which makes the corresponding lines difficult to distinguish.

6 Simulation Results

A series of Monte-Carlo comparison studies were conducted under various conditions, in order to validate the preceding theoretical analysis and to demonstrate the capability of the OC-EKF (1.0 and 2.0) estimators to improve the consistency of EKF-CL. The metrics used to evaluate filter performance are: (i) the average root mean squared (RMS) error, and (ii) the average normalized (state) estimation error squared (NEES) [14]. It is known that the NEES of an M-dimensional Gaussian random variable follows a χ^2 distribution with M degrees of freedom. Therefore, if a certain filter is consistent, we expect that the average NEES for each robot pose will be close to 3 for all k. The larger the deviation of the NEES from these values, the larger the inconsistency of the filter. By studying both the RMS errors and NEES of all the filters considered here, we obtain a comprehensive picture of the estimators' performance.

In the simulation tests, we consider a CL scenario in which four robots move randomly in an area of size 20 m $\times$ 20 m. 50 Monte Carlo simulations were performed, and during each run, all filters process the same data, to ensure a fair comparison. The four estimators compared are:

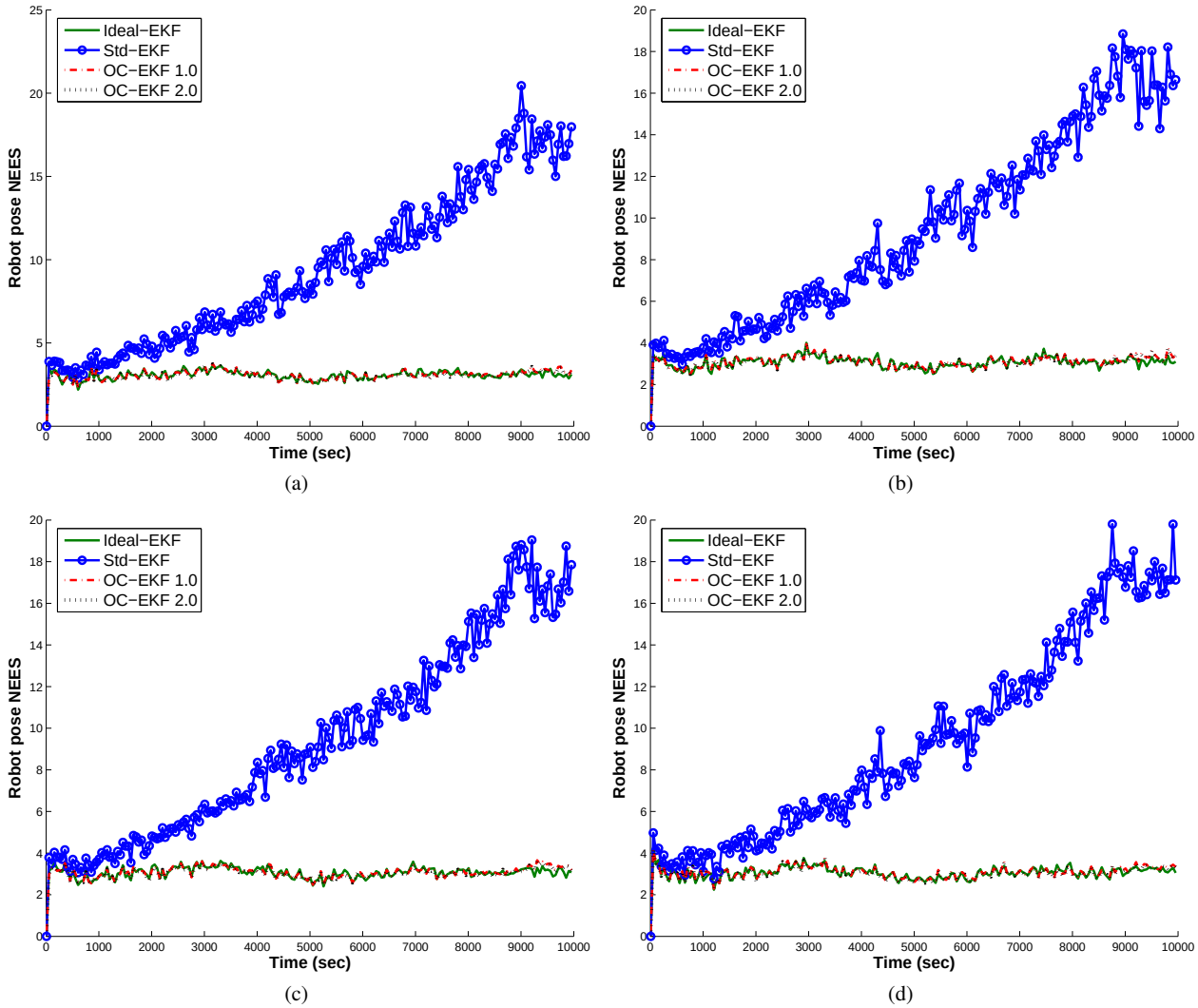

Fig. 2 Monte Carlo simulation results for the average NEES of the robot-pose errors: (a) Robot 1, (b) Robot 2, (c) Robot 3, (d) Robot 4. In these plots, the solid lines correspond to the ideal EKF, the solid lines with circles to the standard EKF, the dash-dotted lines to the OC-EKF 1.0, and the dotted lines to the OC-EKF 2.0. Note that the NEES of the ideal EKF and the OC-EKFs are almost identical, which makes the corresponding lines difficult to distinguish.

(i) the ideal EKF, (ii) the standard EKF, (iii) the OC-EKF 1.0, and (iv) the OC-EKF 2.0.

For the results presented in this section, four identical robots with a simple differential drive model move on a planar surface, at a constant linear velocity of $v = 0.25$ m/sec, while the rotational velocity is drawn from the uniform distribution over $[-0.5, 0.5]$ rad/sec. The two drive wheels are equipped with encoders, which measure their revolutions and provide noisy measurements of velocity (i.e., right and left wheel velocities, v_r and v_l, respectively), with standard deviation equal to $\sigma = 5\%v$ for each wheel. These measurements are used to obtain linear and rotational velocity measurements for each robot, which are given by $v = \frac{v_r+v_l}{2}$ and $\omega = \frac{v_r-v_l}{a}$, where $a = 0.5$ m is the distance between the drive wheels. Thus, the standard deviations of the linear and rotational velocity measurements are $\sigma_v = \frac{\sqrt{2}}{2}\sigma$ and $\sigma_\omega = \frac{\sqrt{2}}{a}\sigma$, respectively.

Each robot records distance and bearing measurements to all other robots. Note that for simplicity we assume that all measurements occur at every time step in our simulations (but this is not the case in our real-world experiments in Section 7). The standard deviation of the distance measurement noise is equal to 10% of the robot-to-robot distance, while the standard deviation of the bearing measurement noise is set to $\sigma_\theta = 10$ deg. It should be pointed out that the sensor-noise levels selected for the simulations are larger than what is typically encountered in practice. This was done purposefully, since larger noise levels lead to higher estimation errors, which make the effects of inconsistency more apparent.

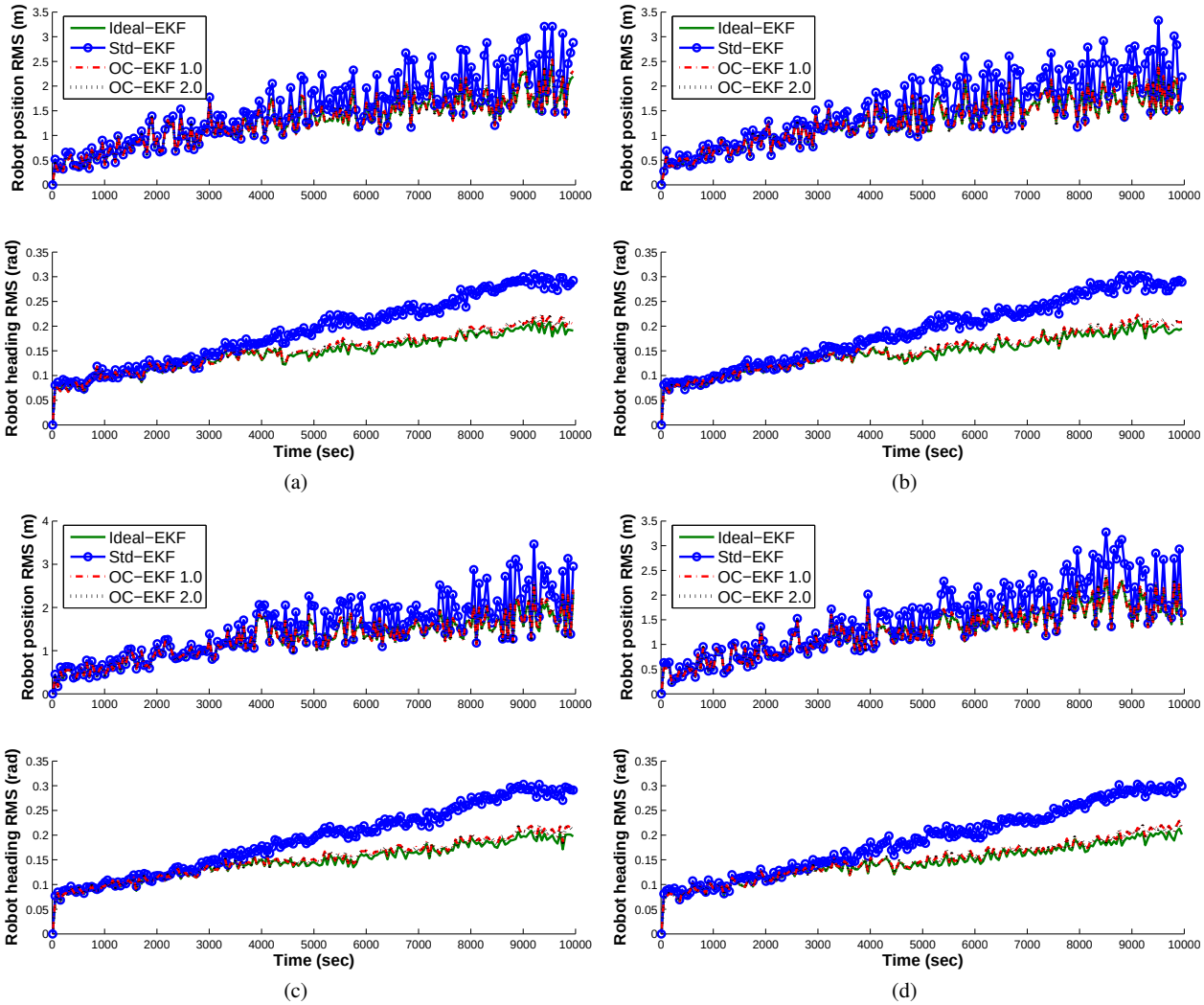

Fig. 3 Monte Carlo simulation results for the average RMS of the robot pose errors: (a) Robot 1, (b) Robot 2, (c) Robot 3, (d) Robot 4. In these plots, the solid lines correspond to the ideal EKF, the solid lines with circles to the standard EKF, the dash-dotted lines to the OC-EKF 1.0, and the dotted lines to the OC-EKF 2.0. Note that the RMS errors of the ideal EKF and the OC-EKFs are almost identical, which makes the corresponding lines difficult to distinguish.

Fig. 1 shows the orientation estimation errors for one of the robots, obtained from a typical simulation (the results for the other three robots are very similar and thus omitted for clarity). Clearly, the standard-EKF errors grow significantly faster than those of the ideal EKF and the OC-EKFs, which indicates that the standard EKF tends to diverge. Note also that although the orientation errors of the ideal EKF and the OC-EKFs remain well within their corresponding 3σ bounds, those of the standard EKF exceed them. Most importantly, in contrast to those of the OC-EKFs, the 3σ bounds of the standard EKF (computed from the square-root of the corresponding element of the estimated covariance matrix) remain almost *constant* as if the orientation of the robot was observable. However, as discussed in Section 4, the robots have no access to absolute orientation information and thus the orientation covariance should continuously grow (as is the case for the ideal EKF and the OC-EKFs). The results of Fig. 1 clearly demonstrate that the incorrect observability properties of the standard EKF cause an unjustified reduction of the orientation uncertainty.

Figs. 2 and 3 show the average NEES and RMS errors, respectively, for all four robots. These plots show the average errors over all Monte Carlo runs, plotted over time, while Table 1 presents the average error values over all time steps. As evident, the performance of both the OC-EKFs is *almost identical* to that of the ideal EKF, and substantially better than the standard EKF, both in terms of RMS errors and NEES. This occurs even though the Jacobians used in the OC-EKFs are less accurate than those used in the standard EKF, as explained in the preceding section. This fact indicates that the errors introduced by the use of inaccurate Jacobians have a less detrimental effect on consistency than

	Ideal-EKF	Std-EKF	OC-EKF 1.0	OC-EKF 2.0
Robot Position Err. RMS (m)				
Robot 1:	1.2820	1.5062	1.2927	1.2912
Robot 2:	1.2747	1.5022	1.2857	1.2844
Robot 3:	1.2723	1.4966	1.2830	1.2818
Robot 4:	1.2721	1.4990	1.2808	1.2793
Robot Heading Err. RMS (rad)				
Robot 1:	0.1455	0.1908	0.1497	0.1494
Robot 2:	0.1454	0.1906	0.1495	0.1492
Robot 3:	0.1455	0.1908	0.1497	0.1494
Robot 4:	0.1453	0.1906	0.1495	0.1492
Robot Pose NEES				
Robot 1:	3.0690	9.4293	3.0825	3.0485
Robot 2:	3.0626	9.4087	3.0953	3.0617
Robot 3:	3.0699	9.4214	3.0855	3.0512
Robot 4:	3.0767	9.4596	3.0911	3.0561

Table 1 Robot pose estimation performance in the simulation

	Std-EKF	OC-EKF 1.0	OC-EKF 2.0
Robot Position Err. RMS (m)			
Robot 1:	0.2132	0.1070	0.1066
Robot 2:	0.2127	0.1083	0.1080
Robot 3:	0.2104	0.1076	0.1073
Robot 4:	0.2699	0.1317	0.1313
Robot Heading Err. RMS (rad)			
Robot 1:	0.1721	0.0785	0.0782
Robot 2:	0.1694	0.0760	0.0757
Robot 3:	0.1732	0.0794	0.0791
Robot 4:	0.1749	0.0810	0.0807
Robot Pose NEES			
Robot 1:	24.2458	4.4080	4.4289
Robot 2:	26.4881	4.5423	4.5801
Robot 3:	25.3439	4.6060	4.6270
Robot 4:	27.6313	4.9182	4.9501

Table 2 Robot pose estimation performance in the experiment

the use of an error-state system model with observable subspace of dimension larger than that of the actual CL system. In addition, the performance of the OC-EKF 2.0 is superior to that of the OC-EKF 1.0 by a small margin. This is attributed to the fact that the OC-EKF 1.0 has larger linearization errors than its alternative, the OC-EKF 2.0, whose linearization errors are optimal by construction, under the observability constraints. We have also tested the performance of our proposed estimators for varying team sizes, with very similar results to the ones shown for the four-robot case. We omit the results here, but the interested reader is referred to [37] for details.

7 Experimental Results

In what follows, we describe one of the real-world experiments performed to further validate the OC-EKF algorithms. During the test, a team of four Pioneer I robots moves in a rectangular area of 2.5 m $\times$ 4.5 m, within which the positions of the robots are being tracked by an overhead camera. For this purpose, rectangular targets are mounted on top of the robots and the vision system is calibrated in order to provide ground-truth measurements of the robots' poses in a global coordinate frame. The standard deviation of the noise in these measurements is approximately 0.5 deg for orientation and 0.01 m, along each axis, for position. The robots were commanded to move at a constant velocity of $v = 0.1$ m/sec while avoiding collision with the boundaries of the arena as well as with their teammates. Fig. 4(a) shows the experimental setup. The trajectories of the four robots are shown in Fig. 4(b), where only partial trajectories are plotted in order to keep the figure clear.

Although four identical robots were used, calibration of their odometric sensors showed that the accuracy of the wheel-encoders' measurements is not identical for all robots. Specifically, the measurement errors are well-modeled as Gaussian zero-mean white noise processes and the standard deviation of the velocity measurements ranges from $\sigma_{v_{\min}} = 3.8\%v$ for the most accurate odometer to $\sigma_{v_{\max}} = 6.9\%v$ for the robot with the highest noise levels. Similarly, the standard deviations of the rotational velocity measurements have values between $\sigma_{\omega_{\min}} = 0.0078$ rad/sec and $\sigma_{\omega_{\max}} = 0.02$ rad/sec for the four robots. We observe that as a result of the variability of sensor characteristics, attributed to manufacturing imperfections, the experiment involves a *heterogeneous* robot team, despite all robots being the same model, equipped with the same sensors. This gives us the opportunity to test the performance of the OC-EKF algorithms in a realistic scenario. We stress that the derivations of the OC-EKFs in Section 5 require neither the homogeneity of robot teams, nor a complete RMG at every time step. Besides the previous simulations in which a homogeneous robot team was used, this experiment demonstrates the superior performance of the OC-EKFs versus the standard EKF also for heterogeneous robot teams.

Relative distance-bearing measurements are produced synthetically using the differences in the positions of the robots, as these are recorded by the overhead camera, with the addition of noise. For the experimental results shown in this section, the distance and bearing measurements are corrupted by zero-mean white Gaussian noise processes, with standard deviation $\sigma_d = 0.05$ m and $\sigma_\theta = 2$ deg, respectively.

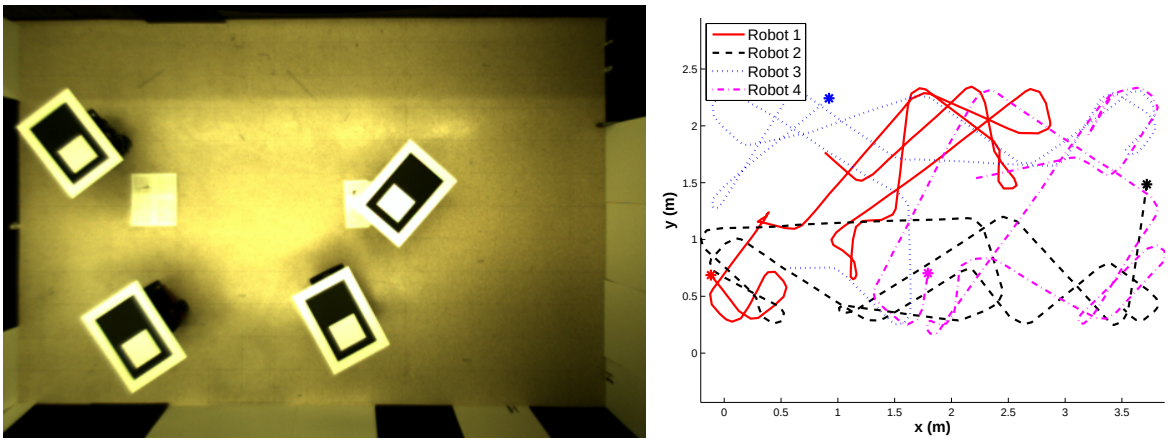

(a) (b)

Fig. 4 Experimental setup: (a) Calibrated image of four Pioneer I robots with targets mounted on top of them. (b) Trajectories of four Pioneer I robots that move inside a 2.5 m $\times$ 4.5 m arena during the indoor experiment. For presentation clarity, only the parts of the trajectories corresponding to the first 200 sec are plotted. Starting positions are marked by $*$.

Three filters were implemented: (i) the standard EKF, (ii) the OC-EKF 1.0, and (iii) the OC-EKF 2.0. Comparative results for the three filters are presented in Figs. 5 and 6, while Table 2 shows the averaged NEES and RMS errors of the robot pose, respectively. From the experimental results it becomes clear that the two OC-EKFs outperform the standard EKF, in terms of both accuracy and consistency, while both perform almost identically. This agrees with the simulation results presented in the preceding section. Both the real-world and simulation results thus support our conjecture, which states that the mismatch in the dimension of the unobservable subspace between the linearized CL system and the underlying nonlinear system is a fundamental cause of filter inconsistency.

8 Conclusions and Future Work

In this paper, we have studied in depth the issue of consistency in EKF-based CL, from an observability perspective. By comparing the observability properties of the linearized error-state model employed in the EKF with those of the underlying nonlinear CL system, we proved that the observable subspace of the standard EKF system model is always of higher dimension than that of the actual CL system. As a result, the covariance estimates of the EKF undergo reduction in directions of the state space where no information is available, and thus the standard EKF-CL is inconsistent. Moreover, based on the analysis, we proposed two new observability-constrained consistent EKF estimators, the OC-EKF 1.0 and its alternative, OC-EKF 2.0, both of which significantly improve the consistency of EKF-CL. The design methodology followed for deriving the OC-EKFs is based on appropriate selection of the linearization points at which the Jacobians are evaluated, to ensure that the observable subspace of the linearized error-state system model is of the same dimension as that of the underlying nonlinear system. Extensive simulation tests and real-world experiments have verified that the proposed OC-EKFs perform better, in terms of both accuracy and consistency, than the standard EKF.

In this paper, we have focused on 2D CL. However, our approach is also applicable to the case of 3D localization. The details of the application of the proposed design methodology to 3D CL will be the focus of our future work.

A Proof of Lemma 44

In the general case where $N > 2$ robots comprise the team, proceeding similarly to the analysis of the ideal EKF-CL (see Section 4.1.2), the observability matrix $\mathbf{M}$ can be obtained as shown in (67).

Analogously to the proof of Lemma 42, we denote $\mathbf{U} \triangleq \begin{bmatrix}\mathbf{u}_1 & \cdots & \mathbf{u}_{3N}\end{bmatrix}$, and observe that

$$\mathbf{u}_1 = -\sum_{i=2}^{N} \mathbf{u}_{3i-2}\,, \quad \mathbf{u}_2 = -\sum_{i=2}^{N} \mathbf{u}_{3i-1}$$

while

$$\sum_{i=1}^{N} \mathbf{u}_{3i} \neq \sum_{i=2}^{N} \alpha_{2i-1}\mathbf{u}_{3i-2} + \sum_{i=2}^{N} \alpha_{2i}\mathbf{u}_{3i-1}$$

where $\begin{bmatrix}\alpha_{2i-1} \\ \alpha_{2i}\end{bmatrix} \triangleq -\mathbf{J}\boldsymbol{\delta}\hat{\mathbf{p}}_{i1}(k_o,k_o), \forall i = 2,\ldots,N$. This is due to that fact that $\mathbf{u}_{3i}$, $i = 1,\ldots,N$, become general vectors and hence are no longer linear combinations of any other columns. This is in contrast to the case of the ideal EKF-CL (see Lemma 42). As a result, one possible basis of the range of matrix $\mathbf{U}$ is its column vectors $\{\mathbf{u}_i\}_{i=3}^{3N}$, i.e., $\mathrm{rng}(\mathbf{U}) = \underset{\text{col.}}{\mathrm{span}}\begin{bmatrix}\mathbf{u}_3 & \cdots & \mathbf{u}_{3N}\end{bmatrix}$. Thus, $\mathrm{rank}(\mathbf{U}) = 3N-2$. Analogously, we observe that in general $\mathbf{D}\mathbf{u}_i \neq \mathbf{0}$, for $i = 3,\ldots,3N$. Moreover, note that any vector $\mathbf{x} \in \mathrm{rng}(\mathbf{U}) \setminus \mathbf{0}$ can be written as $\mathbf{x} = \sum_{i=1}^{3N-2} \beta_i \mathbf{u}_{i+2}$ for some $\beta_i \in \mathbb{R}$, where β_i's are not simultaneously equal to zero.

$$\mathbf{M} = \underbrace{-\mathbf{Diag}\left((\nabla\mathbf{h}_{k_o}^{(12)})\mathbf{A}(\hat{\phi}_{1_{k_o|k_o-1}}),\ \cdots,\ (\nabla\mathbf{h}_{k_o+m}^{(NN-1)})\mathbf{A}(\hat{\phi}_{N_{k_o+m|k_o+m-1}})\right)}_{\mathbf{D}} \times \tag{67}$$

$$\underbrace{\begin{bmatrix}
\mathbf{I}_2 & \mathbf{J\delta\hat{p}}_{21}(k_o,k_o) & -\mathbf{I}_2 & \mathbf{0}_{2\times1} & \mathbf{0}_{2\times2} & \cdots & \mathbf{0}_{2\times2} & \mathbf{0}_{2\times1} \\
\mathbf{0}_{1\times2} & 1 & \mathbf{0}_{1\times2} & -1 & \mathbf{0}_{1\times2} & \cdots & \mathbf{0}_{1\times2} & 0 \\
\mathbf{I}_2 & \mathbf{J\delta\hat{p}}_{31}(k_o,k_o) & \mathbf{0}_{2\times2} & \mathbf{0}_{2\times1} & -\mathbf{I}_2 & \cdots & \mathbf{0}_{2\times2} & \mathbf{0}_{2\times1} \\
\mathbf{0}_{1\times2} & 1 & \mathbf{0}_{1\times2} & 0 & \mathbf{0}_{1\times2} & \cdots & \mathbf{0}_{1\times2} & 0 \\
\vdots & \vdots & \vdots & \vdots & \vdots & \ddots & \vdots & \vdots \\
\mathbf{I}_2 & \mathbf{J\delta\hat{p}}_{N1}(k_o,k_o) & \mathbf{0}_{2\times2} & \mathbf{0}_{2\times1} & \mathbf{0}_{2\times2} & \cdots & -\mathbf{I}_2 & \mathbf{0}_{2\times1} \\
\mathbf{0}_{1\times2} & 1 & \mathbf{0}_{1\times2} & 0 & \mathbf{0}_{1\times2} & \cdots & \mathbf{0}_{1\times2} & -1 \\
\vdots & \vdots & \vdots & \vdots & \vdots & \vdots & \vdots & \vdots \\
-\mathbf{I}_2 & \mathbf{0}_{2\times1} & \mathbf{0}_{2\times2} & \mathbf{0}_{2\times1} & \mathbf{0}_{2\times2} & \cdots & \mathbf{I}_2 & \mathbf{J\delta\hat{p}}_{1N}(k_o,k_o) \\
\mathbf{0}_{1\times2} & -1 & \mathbf{0}_{1\times2} & 0 & \mathbf{0}_{1\times2} & \cdots & \mathbf{0}_{1\times2} & 1 \\
\mathbf{0}_{2\times2} & \mathbf{0}_{2\times1} & -\mathbf{I}_2 & \mathbf{0}_{2\times1} & \mathbf{0}_{2\times2} & \cdots & \mathbf{I}_2 & \mathbf{J\delta\hat{p}}_{2N}(k_o,k_o) \\
\mathbf{0}_{1\times2} & 0 & \mathbf{0}_{1\times2} & -1 & \mathbf{0}_{1\times2} & \cdots & \mathbf{0}_{1\times2} & 1 \\
\vdots & \vdots & \vdots & \vdots & \vdots & \ddots & \vdots & \vdots \\
\mathbf{0}_{2\times2} & \mathbf{0}_{2\times1} & \mathbf{0}_{2\times2} & \mathbf{0}_{2\times1} & \mathbf{0}_{2\times2} & \cdots & \mathbf{I}_2 & \mathbf{J\delta\hat{p}}_{N-1N}(k_o,k_o) \\
\mathbf{0}_{1\times2} & 0 & \mathbf{0}_{1\times2} & 0 & \mathbf{0}_{1\times2} & \cdots & \mathbf{0}_{1\times2} & 1 \\
\mathbf{I}_2 & \mathbf{J\Delta\hat{p}}_{21}(k_o+1,k_o) & -\mathbf{I}_2 & -\mathbf{J\Delta\hat{p}}_{22}(k_o+1,k_o) & \mathbf{0}_{2\times2} & \cdots & \mathbf{0}_{2\times2} & \mathbf{0}_{2\times1} \\
\mathbf{0}_{1\times2} & 1 & \mathbf{0}_{1\times2} & -1 & \mathbf{0}_{1\times2} & \cdots & \mathbf{0}_{1\times2} & 0 \\
\mathbf{I}_2 & \mathbf{J\Delta\hat{p}}_{31}(k_o+1,k_o) & \mathbf{0}_{2\times2} & \mathbf{0}_{2\times1} & -\mathbf{I}_2 & -\mathbf{J\Delta\hat{p}}_{33}(k_o+1,k_o) & \cdots & \mathbf{0}_{2\times2} & \mathbf{0}_{2\times1} \\
\mathbf{0}_{1\times2} & 1 & \mathbf{0}_{1\times2} & 0 & \mathbf{0}_{1\times2} & -1 & \cdots & \mathbf{0}_{1\times2} & 0 \\
\vdots & \vdots & \vdots & \vdots & \vdots & \vdots & \ddots & \vdots & \vdots \\
\mathbf{I}_2 & \mathbf{J\Delta\hat{p}}_{N1}(k_o+1,k_o) & \mathbf{0}_{2\times2} & \mathbf{0}_{2\times1} & \mathbf{0}_{2\times2} & \mathbf{0}_{2\times1} & \cdots & -\mathbf{I}_2 & -\mathbf{J\Delta\hat{p}}_{NN}(k_o+1,k_o) \\
\mathbf{0}_{1\times2} & 1 & \mathbf{0}_{1\times2} & 0 & \mathbf{0}_{1\times2} & 0 & \cdots & \mathbf{0}_{1\times2} & -1 \\
\vdots & \vdots & \vdots & \vdots & \vdots & \vdots & \vdots & \vdots & \vdots \\
-\mathbf{I}_2 & -\mathbf{J\Delta\hat{p}}_{11}(k_o+1,k_o) & \mathbf{0}_{2\times2} & \mathbf{0}_{2\times1} & \mathbf{0}_{2\times2} & \mathbf{0}_{2\times1} & \cdots & \mathbf{I}_2 & \mathbf{J\Delta\hat{p}}_{1N}(k_o+1,k_o) \\
\mathbf{0}_{1\times2} & -1 & \mathbf{0}_{1\times2} & 0 & \mathbf{0}_{1\times2} & 0 & \cdots & \mathbf{0}_{1\times2} & 1 \\
\mathbf{0}_{2\times2} & \mathbf{0}_{2\times1} & -\mathbf{I}_2 & -\mathbf{J\Delta\hat{p}}_{22}(k_o+1,k_o) & \mathbf{0}_{2\times2} & \mathbf{0}_{2\times1} & \cdots & \mathbf{I}_2 & \mathbf{J\Delta\hat{p}}_{2N}(k_o+1,k_o) \\
\mathbf{0}_{1\times2} & 0 & \mathbf{0}_{1\times2} & -1 & \mathbf{0}_{1\times2} & 0 & \cdots & \mathbf{0}_{1\times2} & 1 \\
\vdots & \vdots & \vdots & \vdots & \vdots & \vdots & \ddots & \vdots & \vdots \\
\mathbf{0}_{2\times2} & \mathbf{0}_{2\times1} & \mathbf{0}_{2\times2} & \mathbf{0}_{2\times1} & \mathbf{0}_{2\times2} & \mathbf{0}_{2\times1} & \cdots & \mathbf{I}_2 & \mathbf{J\Delta\hat{p}}_{N-1N}(k_o+1,k_o) \\
\mathbf{0}_{1\times2} & 0 & \mathbf{0}_{1\times2} & 0 & \mathbf{0}_{1\times2} & 0 & \cdots & \mathbf{0}_{1\times2} & 1 \\
\mathbf{I}_2 & \mathbf{J\Delta\hat{p}}_{21}(k_o+m,k_o+m-1) & -\mathbf{I}_2 & -\mathbf{J\Delta\hat{p}}_{22}(k_o+m,k_o+m-1) & \mathbf{0}_{2\times2} & \cdots & \mathbf{0}_{2\times2} & \mathbf{0}_{2\times1} \\
\mathbf{0}_{1\times2} & 1 & \mathbf{0}_{1\times2} & -1 & \mathbf{0}_{1\times2} & \cdots & \mathbf{0}_{1\times2} & 0 \\
\mathbf{I}_2 & \mathbf{J\Delta\hat{p}}_{31}(k_o+m,k_o+m-1) & \mathbf{0}_{2\times2} & \mathbf{0}_{2\times1} & -\mathbf{I}_2 & -\mathbf{J\Delta\hat{p}}_{33}(k_o+m,k_o+m-1) & \cdots & \mathbf{0}_{2\times2} & \mathbf{0}_{2\times1} \\
\mathbf{0}_{1\times2} & 1 & \mathbf{0}_{1\times2} & 0 & \mathbf{0}_{1\times2} & -1 & \cdots & \mathbf{0}_{1\times2} & 0 \\
\vdots & \vdots & \vdots & \vdots & \vdots & \vdots & \ddots & \vdots & \vdots \\
\mathbf{I}_2 & \mathbf{J\Delta\hat{p}}_{N1}(k_o+m,k_o+m-1) & \mathbf{0}_{2\times2} & \mathbf{0}_{2\times1} & \mathbf{0}_{2\times2} & \mathbf{0}_{2\times1} & \cdots & -\mathbf{I}_2 & -\mathbf{J\Delta\hat{p}}_{NN}(k_o+m,k_o+m-1) \\
\mathbf{0}_{1\times2} & 1 & \mathbf{0}_{1\times2} & 0 & \mathbf{0}_{1\times2} & 0 & \cdots & \mathbf{0}_{1\times2} & -1 \\
\vdots & \vdots & \vdots & \vdots & \vdots & \vdots & \vdots & \vdots & \vdots \\
-\mathbf{I}_2 & -\mathbf{J\Delta\hat{p}}_{11}(k_o+m,k_o+m-1) & \mathbf{0}_{2\times2} & \mathbf{0}_{2\times1} & \mathbf{0}_{2\times2} & \mathbf{0}_{2\times1} & \cdots & \mathbf{I}_2 & \mathbf{J\Delta\hat{p}}_{1N}(k_o+m,k_o+m-1) \\
\mathbf{0}_{1\times2} & -1 & \mathbf{0}_{1\times2} & 0 & \mathbf{0}_{1\times2} & 0 & \cdots & \mathbf{0}_{1\times2} & 1 \\
\mathbf{0}_{2\times2} & \mathbf{0}_{2\times1} & -\mathbf{I}_2 & -\mathbf{J\Delta\hat{p}}_{22}(k_o+m,k_o+m-1) & \mathbf{0}_{2\times2} & \mathbf{0}_{2\times1} & \cdots & \mathbf{I}_2 & \mathbf{J\Delta\hat{p}}_{2N}(k_o+m,k_o+m-1) \\
\mathbf{0}_{1\times2} & 0 & \mathbf{0}_{1\times2} & -1 & \mathbf{0}_{1\times2} & 0 & \cdots & \mathbf{0}_{1\times2} & 1 \\
\vdots & \vdots & \vdots & \vdots & \vdots & \vdots & \ddots & \vdots & \vdots \\
\mathbf{0}_{2\times2} & \mathbf{0}_{2\times1} & \mathbf{0}_{2\times2} & \mathbf{0}_{2\times1} & \mathbf{0}_{2\times2} & \mathbf{0}_{2\times1} & \cdots & \mathbf{I}_2 & \mathbf{J\Delta\hat{p}}_{N-1N}(k_o+m,k_o+m-1) \\
\mathbf{0}_{1\times2} & 0 & \mathbf{0}_{1\times2} & 0 & \mathbf{0}_{1\times2} & 0 & \cdots & \mathbf{0}_{1\times2} & 1
\end{bmatrix}}_{\mathbf{U}}$$

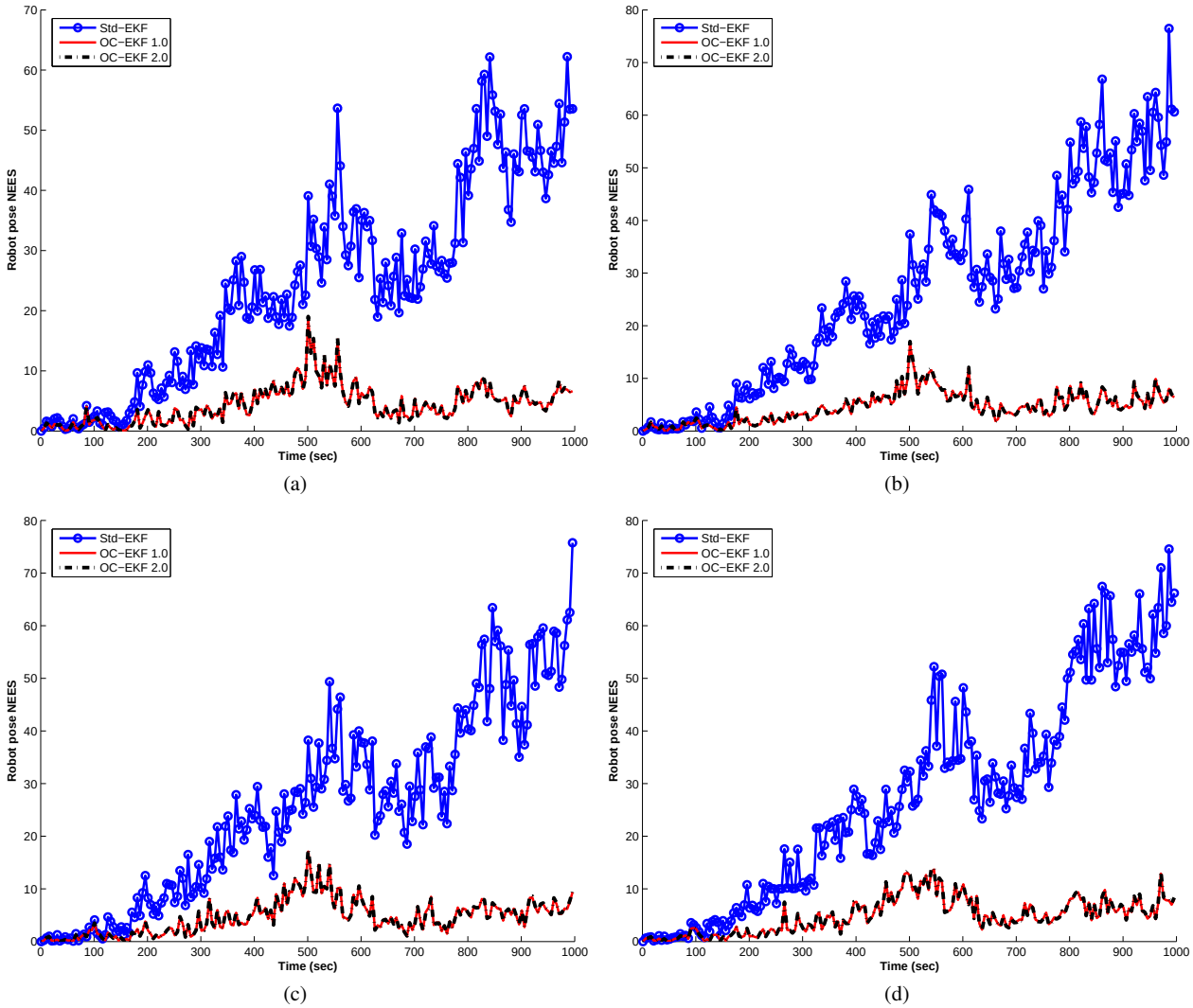

Fig. 5 Experimental results for the NEES of the robot pose errors: (a) Robot 1, (b) Robot 2, (c) Robot 3, (d) Robot 4. In these plots, the solid lines with circles correspond to the standard EKF, the solid lines to the OC-EKF 1.0, and the dash-dotted lines to the OC-EKF 2.0. Note that the NEES of the two OC-EKFs are almost identical, which makes the corresponding lines difficult to distinguish.

Thus, we see that in general $\mathbf{Dx} = \sum_{i=1}^{3N-2} \beta_i \mathbf{D}\mathbf{u}_{i+2} \neq \mathbf{0}$, which implies that $\mathbf{x}$ does not belong to the null space, null($\mathbf{D}$), of $\mathbf{D}$. Therefore, $\dim(\text{null}(\mathbf{D}) \bigcap \text{rng}(\mathbf{U})) = 0$, and, finally, based on theorem (4.5.1) in [36], $\text{rank}(\mathbf{M}) = \text{rank}(\mathbf{U}) - \dim(\text{null}(\mathbf{D}) \bigcap \text{rng}(\mathbf{U})) = \text{rank}(\mathbf{U}) = 3N-2$.

B Proof of Lemma 53

Under the Gaussianity assumption, it is $p(\mathbf{x}_k|\mathbf{z}_{0:k}) = \mathcal{N}(\hat{\mathbf{x}}_{k|k}, \mathbf{P}_{k|k})$, and $p(\mathbf{x}_{k+1}|\mathbf{z}_{0:k}) = \mathcal{N}(\hat{\mathbf{x}}_{k+1|k}, \mathbf{P}_{k+1|k})$. The first term of the cost function (53) is computed as

$$
\begin{aligned}
&\int \left\|\mathbf{x}_k - \mathbf{x}_{k|k}^\star\right\|^2 p(\mathbf{x}_k|\mathbf{z}_{0:k}) d\mathbf{x}_k \\
&= \int \left(\mathbf{x}_k^T\mathbf{x}_k - 2\mathbf{x}_k^T\mathbf{x}_{k|k}^\star + \mathbf{x}_{k|k}^{\star T}\mathbf{x}_{k|k}^\star\right) p(\mathbf{x}_k|\mathbf{z}_{0:k}) d\mathbf{x}_k \\
&= \mathbb{E}\left(\mathbf{x}_k^T\mathbf{x}_k|\mathbf{z}_{0:k}\right) - 2\mathbb{E}\left(\mathbf{x}_k^T|\mathbf{z}_{0:k}\right)\mathbf{x}_{k|k}^\star + \mathbf{x}_{k|k}^{\star T}\mathbf{x}_{k|k}^\star \\
&= \text{tr}\left(\mathbf{P}_{k|k} + \hat{\mathbf{x}}_{k|k}\hat{\mathbf{x}}_{k|k}^T\right) - 2\hat{\mathbf{x}}_{k|k}^T\mathbf{x}_{k|k}^\star + \mathbf{x}_{k|k}^{\star T}\mathbf{x}_{k|k}^\star \\
&= \text{tr}\left(\mathbf{P}_{k|k}\right) + \hat{\mathbf{x}}_{k|k}^T\hat{\mathbf{x}}_{k|k} - 2\hat{\mathbf{x}}_{k|k}^T\mathbf{x}_{k|k}^\star + \mathbf{x}_{k|k}^{\star T}\mathbf{x}_{k|k}^\star \\
&= \text{tr}\left(\mathbf{P}_{k|k}\right) + \left\|\hat{\mathbf{x}}_{k|k} - \mathbf{x}_{k|k}^\star\right\|^2
\end{aligned} \tag{68}
$$

where $\mathbb{E}(\cdot)$ denotes expectation and $\text{tr}(\cdot)$ is the matrix trace. Proceeding similarly, the second term of the cost function (53) can be derived as

$$
\begin{aligned}
&\int \left\|\mathbf{x}_{k+1} - \mathbf{x}_{k+1|k}^\star\right\|^2 p(\mathbf{x}_{k+1}|\mathbf{z}_{0:k}) d\mathbf{x}_{k+1} \\
&= \text{tr}\left(\mathbf{P}_{k+1|k}\right) + \left\|\hat{\mathbf{x}}_{k+1|k} - \mathbf{x}_{k+1|k}^\star\right\|^2
\end{aligned} \tag{69}
$$

Using (68) and (69), as well as the fact that the true $\mathbf{P}_{k|k}$ and $\mathbf{P}_{k+1|k}$ are independent of the linearization points, the following equivalence holds:

$$
\begin{aligned}
&\min_{\mathbf{x}_{k|k}^\star,\, \mathbf{x}_{k+1|k}^\star} \left\{ \begin{array}{l} \text{tr}\left(\mathbf{P}_{k|k}\right) + \text{tr}\left(\mathbf{P}_{k+1|k}\right) + \\ \left\|\hat{\mathbf{x}}_{k|k} - \mathbf{x}_{k|k}^\star\right\|^2 + \left\|\hat{\mathbf{x}}_{k+1|k} - \mathbf{x}_{k+1|k}^\star\right\|^2 \end{array} \right\} \\
\Leftrightarrow &\min_{\mathbf{x}_{k|k}^\star,\, \mathbf{x}_{k+1|k}^\star} \left\|\hat{\mathbf{x}}_{k|k} - \mathbf{x}_{k|k}^\star\right\|^2 + \left\|\hat{\mathbf{x}}_{k+1|k} - \mathbf{x}_{k+1|k}^\star\right\|^2
\end{aligned} \tag{70}
$$

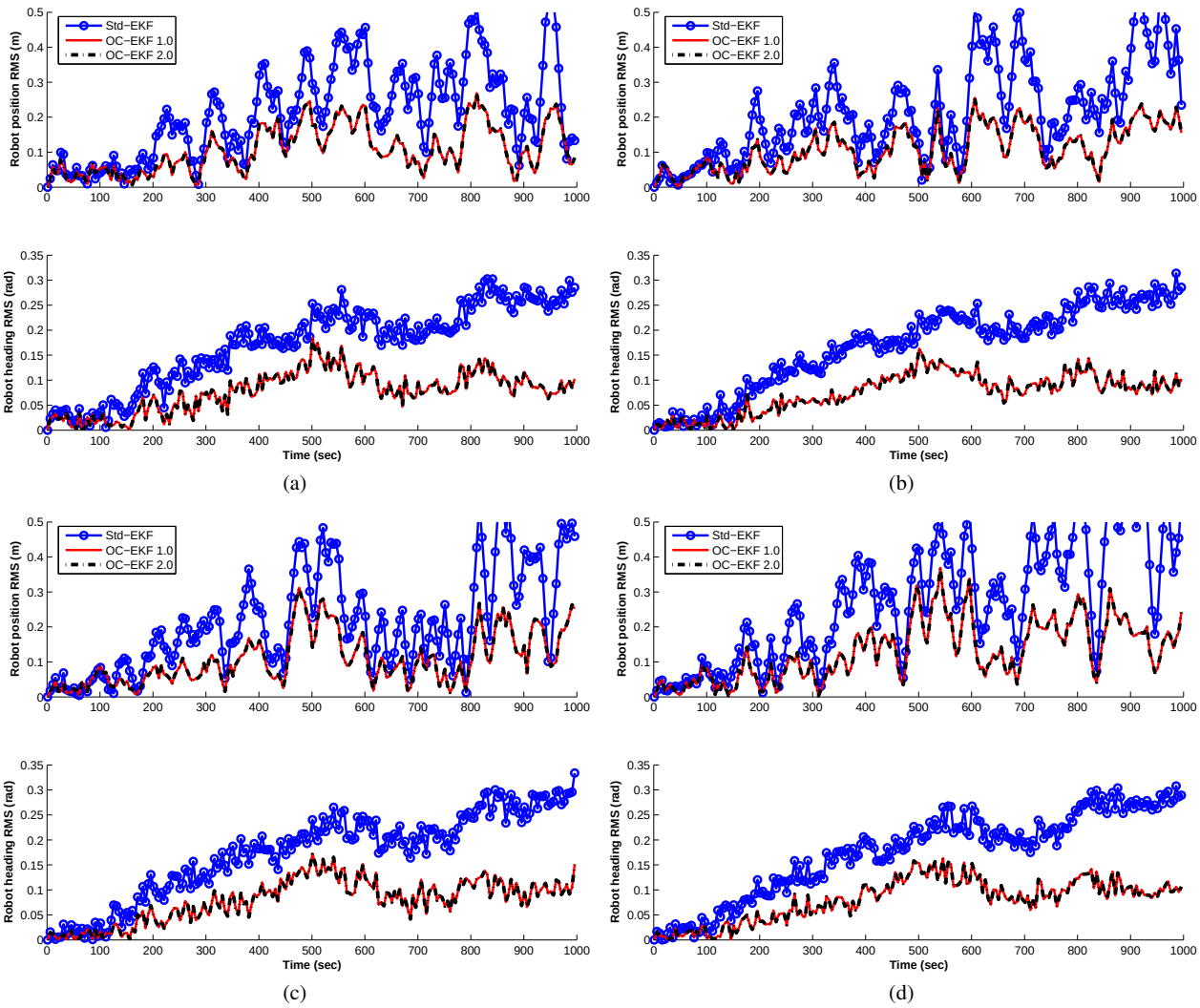

Fig. 6 Experimental results for the robot pose absolute errors: (a) Robot 1, (b) Robot 2, (c) Robot 3, (d) Robot 4. In these plots, the solid lines with circles correspond to the standard EKF, the solid lines to the OC-EKF 1.0, and the dash-dotted lines to the OC-EKF 2.0. Note that the absolute errors of the two OC-EKFs are almost identical, which makes the corresponding lines difficult to distinguish.

We now derive the following identities for the observability constraint (54) (see (42) and (48)):

$$\begin{aligned}
&\mathbf{H}_{k+1}\boldsymbol{\Phi}_k\cdots\boldsymbol{\Phi}_{k_o}\mathbf{N}=\mathbf{0}\\
\Leftrightarrow\ &\sum_{\tau=k_o}^{k}(\mathbf{p}^\star_{2_{\tau|\tau}}-\mathbf{p}^\star_{2_{\tau|\tau-1}})-\sum_{\tau=k_o}^{k}(\mathbf{p}^\star_{1_{\tau|\tau}}-\mathbf{p}^\star_{1_{\tau|\tau-1}})+\\
&\left(\mathbf{p}^\star_{2_{k_o|k_o-1}}-\mathbf{p}^\star_{1_{k_o|k_o-1}}\right)-\left(\hat{\mathbf{p}}_{2_{k_o|k_o-1}}-\hat{\mathbf{p}}_{1_{k_o|k_o-1}}\right)=\mathbf{0} \qquad (71)\\
\Leftrightarrow\ &\mathbf{p}^\star_{2_{k|k}}-\mathbf{p}^\star_{1_{k|k}}=\left(\mathbf{p}^\star_{2_{k|k-1}}-\mathbf{p}^\star_{1_{k|k-1}}\right)-\\
&\sum_{\tau=k_o}^{k-1}(\mathbf{p}^\star_{2_{\tau|\tau}}-\mathbf{p}^\star_{2_{\tau|\tau-1}})+\sum_{\tau=k_o}^{k-1}(\mathbf{p}^\star_{1_{\tau|\tau}}-\mathbf{p}^\star_{1_{\tau|\tau-1}}) \qquad (72)
\end{aligned}$$

where we have used the fact that the linearization points, during propagation at time-step k_o are the propagated filter estimates, i.e., $\mathbf{p}^\star_{1_{k_o|k_o-1}}=\hat{\mathbf{p}}_{1_{k_o|k_o-1}}$ and $\mathbf{p}^\star_{2_{k_o|k_o-1}}=\hat{\mathbf{p}}_{2_{k_o|k_o-1}}$. This completes the proof.

C An Example of OC-EKF CL

In the following, we provide a specific CL example to illustrate the implementation of the proposed OC-EKF estimators, in which a team of two robots using the unicycle motion model measure relative distance and bearing to each other. Note that the same models were used in our simulations (see Section 6).

Suppose that at the first time-step, $k=0$, the robot poses are initialized by $\hat{\mathbf{x}}_{i_{0|0}}$ and $\mathbf{P}_{i_{0|0}}$, for $i=1,2$. Following standard practice, we employ the approximation that the velocity and heading are constant during each propagation interval and thus obtain ${}^k\hat{\mathbf{x}}_{i_{k+1}}=[v_{m_{i,k}}\ \ 0\ \ \omega_{m_{i,k}}]^T\delta t$, where $\mathbf{u}_{m_{i,k}}=[v_{m_{i,k}}\ \ \omega_{m_{i,k}}]^T$ are the linear and rotational velocity measurements, for $i=1,2$, respectively, and δt is the sampling period. Substitution into (2)-(3) yields the following common equations for robot pose propagation:

$$\hat{\mathbf{p}}_{i_{k+1|k}}=\hat{\mathbf{p}}_{i_{k|k}}+\begin{bmatrix}v_{m_{i,k}}\ c\hat{\phi}_{i_{k|k}}\\ v_{m_{i,k}}\ s\hat{\phi}_{i_{k|k}}\end{bmatrix}\delta t \qquad (73)$$

$$\hat{\phi}_{i_{k+1|k}}=\hat{\phi}_{i_{k|k}}+\omega_{m_{i,k}}\delta t \qquad (74)$$

Std-EKF	$\mathbf{\Phi}_{i_k} = \begin{bmatrix} \mathbf{I}_2 & \mathbf{J}\left(\hat{\mathbf{p}}_{i_{k+1\|k}} - \hat{\mathbf{p}}_{i_{k\|k}}\right) \\ \mathbf{0}_{1\times 2} & 1 \end{bmatrix} = \begin{bmatrix} 1 & 0 & -v_{m_{i,k}} s\hat{\phi}_{i_{k\|k}} \delta t \\ 0 & 1 & v_{m_{i,k}} c\hat{\phi}_{i_{k\|k}} \delta t \\ 0 & 0 & 1 \end{bmatrix}$
OC-EKF 1.0	$\mathbf{\Phi}'_{i_k} = \begin{bmatrix} \mathbf{I}_2 & \mathbf{J}\left(\hat{\mathbf{p}}_{i_{k+1\|k}} - \hat{\mathbf{p}}_{i_{k\|k-1}}\right) \\ \mathbf{0}_{1\times 2} & 1 \end{bmatrix}$
OC-EKF 2.0	$\mathbf{\Phi}''_{i_k} = \begin{bmatrix} \mathbf{I}_2 & \mathbf{J}\left(\hat{\mathbf{p}}_{i_{k+1\|k}} - \hat{\mathbf{p}}_{i_{k\|k}} + (-1)^i \frac{\boldsymbol{\lambda}_k}{2}\right) \\ \mathbf{0}_{1\times 2} & 1 \end{bmatrix}$

Table 3 Different state estimates used in computing the state-propagation Jacobian matrix of robot i ($i = 1,2$) at time-step k for the three estimators (i.e., the standard EKF, the OC-EKFs 1.0 and 2.0)

Once the propagated states are computed, we now calculate the state-propagation Jacobian matrix in order to propagate the covariance. It is important to note that this calculation depends on the particular filter used, and is the *only* difference between the three filters (i.e., the standard EKF, the OC-EKF 1.0 and the OC-EKF 2.0) under consideration in this work. Table 3 summarizes how the state-propagation Jacobian matrix is computed for each estimator. Specifically, in contrast to the standard EKF, the OC-EKF 1.0 requires additional storage of the last propagated state estimate $\hat{\mathbf{x}}_{k|k-1}$, while the OC-EKF 2.0 requires an additional variable $\boldsymbol{\lambda}_k$, containing a running sum of all previous state corrections (see (57)). The noise Jacobian $\mathbf{G}_{i_k}$ with respect to the odometry vector $\mathbf{u}_{i_k}$ for both robots is computed according to (8) for all three estimators (by noting that ${}^k\mathbf{x}_{i_{k+1}} = [v_{i_k} \;\; 0 \;\; \omega_{i_k}]^T \delta t$). The measurement equations and the corresponding Jacobians for the distance and bearing measurement model are given by (see (12)-(14)):

$$\mathbf{z}_{k+1}^{(ij)} = \begin{bmatrix} \sqrt{(x_{j_{k+1}} - x_{i_{k+1}})^2 + (y_{j_{k+1}} - y_{i_{k+1}})^2} \\ \text{atan2}\left((y_{j_{k+1}} - y_{i_{k+1}}), (x_{j_{k+1}} - x_{i_{k+1}})\right) - \phi_{i_{k+1}} \end{bmatrix} + \mathbf{v}_{k+1}^{(ij)} \tag{75}$$

$$\begin{aligned} \mathbf{H}_{k+1}^{(ij)} &= \begin{bmatrix} \mathbf{H}_{1_{k+1}}^{(ij)} & \mathbf{H}_{2_{k+1}}^{(ij)} \end{bmatrix} \\ &= -(\nabla \mathbf{h}_{k+1}^{(ij)}) \mathbf{A}(\hat{\phi}_{i_{k+1|k}}) \begin{bmatrix} \mathbf{I}_2 & \mathbf{J}(\hat{\mathbf{p}}_{j_{k+1|k}} - \hat{\mathbf{p}}_{i_{k+1|k}}) & -\mathbf{I}_2 & 0 \\ \mathbf{0}_{1\times 2} & 1 & 0 & -1 \end{bmatrix} \\ &= -\begin{bmatrix} \frac{\left(\hat{\mathbf{p}}_{j_{k+1|k}}^T - \hat{\mathbf{p}}_{i_{k+1|k}}^T\right)\mathbf{C}(\hat{\phi}_{i_{k+1|k}})}{\|\hat{\mathbf{p}}_{j_{k+1|k}} - \hat{\mathbf{p}}_{i_{k+1|k}}\|} & 0 \\ \frac{\left(\hat{\mathbf{p}}_{j_{k+1|k}}^T - \hat{\mathbf{p}}_{i_{k+1|k}}^T\right)\mathbf{C}(\hat{\phi}_{i_{k+1|k}})\mathbf{J}^T}{\|\hat{\mathbf{p}}_{j_{k+1|k}} - \hat{\mathbf{p}}_{i_{k+1|k}}\|^2} & 0 \end{bmatrix} \begin{bmatrix} \mathbf{C}^T(\hat{\phi}_{i_{k+1|k}}) & 0 \\ 0 & 1 \end{bmatrix} \times \\ &\quad \begin{bmatrix} \mathbf{I}_2 & \mathbf{J}(\hat{\mathbf{p}}_{j_{k+1|k}} - \hat{\mathbf{p}}_{i_{k+1|k}}) & -\mathbf{I}_2 & 0 \\ \mathbf{0}_{1\times 2} & 1 & 0 & -1 \end{bmatrix} \\ &= \begin{bmatrix} -\frac{\hat{\mathbf{p}}_{j_{k+1|k}}^T - \hat{\mathbf{p}}_{i_{k+1|k}}^T}{\|\hat{\mathbf{p}}_{j_{k+1|k}} - \hat{\mathbf{p}}_{i_{k+1|k}}\|} & 0 & \frac{\hat{\mathbf{p}}_{j_{k+1|k}}^T - \hat{\mathbf{p}}_{i_{k+1|k}}^T}{\|\hat{\mathbf{p}}_{j_{k+1|k}} - \hat{\mathbf{p}}_{i_{k+1|k}}\|} & 0 \\ \frac{\left(\hat{\mathbf{p}}_{j_{k+1|k}}^T - \hat{\mathbf{p}}_{i_{k+1|k}}^T\right)\mathbf{J}}{\|\hat{\mathbf{p}}_{j_{k+1|k}} - \hat{\mathbf{p}}_{i_{k+1|k}}\|^2} & -1 & -\frac{\left(\hat{\mathbf{p}}_{j_{k+1|k}}^T - \hat{\mathbf{p}}_{i_{k+1|k}}^T\right)\mathbf{J}}{\|\hat{\mathbf{p}}_{j_{k+1|k}} - \hat{\mathbf{p}}_{i_{k+1|k}}\|^2} & 0 \end{bmatrix} \end{aligned} \tag{76}$$

which hold for $i, j = 1,2$ and $i \neq j$, and are also identical for all three estimators. Given these expressions, we proceed to use the standard EKF propagation and update equations.

Acknowledgements This work was supported by the University of Minnesota (DTC), the UCR Bourns College of Engineering, and the National Science Foundation (IIS-0835637, IIS-0643680, IIS-0811946).

References

1. T. L. Huntsberger, A. Trebi-Ollennu, H. Aghazarian, P. S. Schenker, and P. Pirjanian. Distributed control of multi-robot systems engaged in tightly coupled tasks. *Autonomous Robots*, 17(1):79–92, July 2004.
2. A. D. Tews, G. S. Sukhatme, and M. J. Mataric. A multi-robot approach to stealthy navigation in the presence of an observer. In *Proc. IEEE International Conference on Robotics and Automation*, pages 2379–2385, New Orleans, LA, April 26–May 1, 2004.
3. Y. Feng, Z. Zhu, and J. Xiao. Heterogeneous multi-robot localization in unknown 3D space. In *Proc. IEEE/RSJ International Conference on Intelligent Robots and Systems*, pages 4533–4538, Beijing, China, October 9-15, 2006.
4. R. Kurazume and S. Hirose. An experimental study of a cooperative positioning system. *Autonomous Robots*, 8(1):43–52, January 2000.
5. I. M. Rekleitis, G. Dudek, and E. E. Milios. Multi-robot cooperative localization: a study of trade-offs between efficiency and accuracy. In *Proc. IEEE/RSJ International Conference on Intelligent Robots and Systems*, pages 2690–2695, Switzerland, September 30–October 4, 2002.
6. S. I. Roumeliotis and G. A. Bekey. Distributed multirobot localization. *IEEE Transactions on Robotics and Automation*, 18(5):781–795, October 2002.
7. A. Howard, M. J. Mataric, and G. S. Sukhatme. Localization for mobile robot teams using maximum likelihood estimation. In *Proc. IEEE/RSJ International Conference on Intelligent Robots and Systems*, pages 434–439, Lausanne, Switzerland, September 30–October 4, 2002.
8. E. D. Nerurkar, S. I. Roumeliotis, and A. Martinelli. Distributed maximum a posteriori estimation for multi-robot cooperative localization. In *Proc. IEEE International Conference on Robotics and Automation*, pages 1402–1409, Kobe, Japan, May 12–17, 2009.
9. D. Fox, W. Burgard, H. Kruppa, and S. Thrun. A probabilistic approach to collaborative multi-robot localization. *Autonomous Robots*, 8(3):325–344, June 2000.
10. S. Panzieri, F. Pascucci, and R. Setola. Multirobot localization using interlaced extended Kalman filter. In *Proc. IEEE/RSJ International Conference on Intelligent Robots and Systems*, pages 2816–2821, Beijing, China, October 9-15, 2006.
11. N. Karam, F. Chausse, R. Aufrere, and R. Chapuis. Localization of a group of communicating vehicles by state exchange. In *Proc. IEEE/RSJ International Conference on Intelligent Robots and Systems*, pages 519–524, Beijing, China, October 9-15, 2006.
12. A. I. Mourikis and S. I. Roumeliotis. Optimal sensor scheduling for resource-constrained localization of mobile robot formations. *IEEE Transactions on Robotics*, 22(5):917–931, October 2006.
13. A. Martinelli. Improving the precision on multi robot localization by using a series of filters hierarchically distributed. In *Proc. IEEE/RSJ International Conference on Intelligent Robots and Systems*, pages 1053–1058, San Diego, CA, October 29–November 2, 2007.
14. Y. Bar-Shalom, X. R. Li, and T. Kirubarajan. *Estimation with applications to tracking and navigation*. New York: Wiley, 2001.
15. G. P. Huang, N. Trawny, A. I. Mourikis, and S. I. Roumeliotis. On the consistency of multi-robot cooperative localization. In *Proc. Robotics: Science and Systems*, pages 65–72, Seattle, WA, June 28–July 1, 2009.
16. X. S. Zhou and S. I. Roumeliotis. Robot-to-robot relative pose estimation from range measurements. *IEEE Transactions on Robotics*, 24(6):1379–1393, December 2008.
17. N. Trawny, X. S. Zhou, and S. I. Roumeliotis. 3D relative pose estimation from six distances. In *Proc. Robotics: Science and Systems*, pages 233–240, Seattle, WA, June 28–July 1, 2009.
18. N. Trawny, X. S. Zhou, K. Zhou, and S. I. Roumeliotis. Interrobot transformations in 3-D. *IEEE Transactions on Robotics*, 26(2):226–243, April 2010.
19. N. Trawny and S. I. Roumeliotis. On the global optimum of planar, range-based robot-to-robot relative pose estimation. In

Proc. IEEE International Conference on Robotics and Automation, pages 3200–3206, Anchorage, AK, May3–8, 2010.
20. A. Martinelli and R. Siegwart. Observability analysis for mobile robot localization. In *Proc. IEEE/RSJ International Conference on Intelligent Robots and Systems*, pages 1471–1476, Alberta, Canada, August 2-6, 2005.
21. S. I. Roumeliotis and I. M. Rekleitis. Propagation of uncertainty in cooperative multirobot localization: Analysis and experimental results. *Autonomous Robots*, 17(1):41–54, July 2004.
22. A. I. Mourikis and S. I. Roumeliotis. Performance analysis of multirobot cooperative localization. *IEEE Transactions on Robotics*, 22(4):666–681, August 2006.
23. Y. Dieudonne, O. Labbani-Igbida, and F. Petit. Deterministic robot-network localization is hard. *IEEE Transactions on Robotics*, 26(2):331–339, April 2010.
24. S. Julier and J. Uhlmann. A counter example to the theory of simultaneous localization and map building. In *Proc. IEEE International Conference on Robotics and Automation*, pages 4238–4243, Seoul, Korea, May 2001.
25. J. A. Castellanos, J. Neira, and J. Tardos. Limits to the consistency of EKF-based SLAM. In *Proc. 5th IFAC Symposium on Intelligent Autonomous Vehicles*, pages 1244–1249, Lisbon, Portugal, July 2004.
26. T. Bailey, J. Nieto, J. Guivant, M. Stevens, and E. Nebot. Consistency of the EKF-SLAM algorithm. In *Proc. IEEE/RSJ International Conference on Intelligent Robots and Systems*, pages 3562–3568, Beijing, China, October 2006.
27. S. Huang and G. Dissanayake. Convergence analysis for extended Kalman filter based SLAM. In *Proc. IEEE International Conference on Robotics and Automation*, pages 412–417, Orlando, FL, May 2006.
28. S. Huang and G. Dissanayake. Convergence and consistency analysis for extended Kalman filter based SLAM. *IEEE Transactions on Robotics*, 23(5):1036–1049, October 2007.
29. G. P. Huang, A. I. Mourikis, and S. I. Roumeliotis. Analysis and improvement of the consistency of extended Kalman filter-based SLAM. In *Proc. IEEE International Conference on Robotics and Automation*, pages 473–479, Pasadena, CA, May 12–17, 2008.
30. G. P. Huang, A. I. Mourikis, and S. I. Roumeliotis. A first-estimates Jacobian EKF for improving SLAM consistency. In *Proc. 11th International Symposium on Experimental Robotics*, Athens, Greece, July 14–17, 2008.
31. G. P. Huang, A. I. Mourikis, and S. I. Roumeliotis. Observability-based rules for designing consistent EKF SLAM estimators. *International Journal of Robotics Research*, 29(5):502–528, April 2010.
32. A. Bahr, M. R. Walter, and J. J. Leonard. Consistent cooperative localization. In *Proc. IEEE International Conference on Robotics and Automation*, pages 3415–3422, Kobe, Japan, May 12-17, 2009.
33. A. Howard, M. J. Mataric, and G. S. Sukhatme. Putting the 'I' in 'team': an ego-centric approach to cooperative localization. In *Proc. IEEE International Conference on Robotics and Automation*, pages 868–874, Taipei, Taiwan, September 14-19, 2003.
34. R. Hermann and A. Krener. Nonlinear controllability and observability. *IEEE Transactions on Automatic Control*, 22(5):728 – 740, October 1977.
35. Z. Chen, K. Jiang, and J. C. Hung. Local observability matrix and its application to observability analyses. In *Proc. 16th Annual Conference of IEEE*, pages 100–103, Pacific Grove, CA, November 1990.
36. C. Meyer. *Matrix Analysis and Applied Linear Algebra*. SIAM, 2001.
37. G. P. Huang, N. Trawny, A. I. Mourikis, and S. I. Roumeliotis. On the consistency of multi-robot cooperative localization. Technical report, MARS Lab, University of Minnesota, Minneapolis, MN, January 2009.
38. D. P. Bertsekas. *Nonlinear Programming*. Athena Scientific, 1999.